JPRS L/8683

26 September 1979

USSR Report

PHYSICS AND MATHEMATICS

(FOUO 2/79)

Quantum Electronics

FBIS FOREIGN BROADCAST INFORMATION SERVICE

NOTE

JPRS publications contain information primarily from foreign newspapers, periodicals and books, but also from news agency transmissions and broadcasts. Materials from foreign-language sources are translated; those from English-language sources are transcribed or reprinted, with the original phrasing and other characteristics retained.

Headlines, editorial reports, and material enclosed in brackets [] are supplied by JPRS. Processing indicators such as [Text] or [Excerpt] in the first line of each item, or following the last line of a brief, indicate how the original information was processed. Where no processing indicator is given, the information was summarized or extracted.

Unfamiliar names rendered phonetically or transliterated are enclosed in parentheses. Words or names preceded by a question mark and enclosed in parentheses were not clear in the original but have been supplied as appropriate in context. Other unattributed parenthetical notes within the body of an item originate with the source. Times within items are as given by source.

The contents of this publication in no way represent the policies, views or attitudes of the U.S. Government.

For further information on report content call (703) 351-2938 (economic); 3468 (political, sociological, military); 2726 (life sciences); 2725 (physical sciences).

APPROVED FOR RELEASE: 2007/02/08: CIA-RDP82-00850R000100090042-5

JPRS L/8683

26 September 1979

USSR REPORT

PHYSICS AND MATHEMATICS

(FOUO 2/79)

QUANTUM ELECTRONICS

Moscow KVANTOVAYA ELEKTRONIKA in Russian Vol 6 No. 6(84), Jun 79
pp 1125-1147, 1164-1175, 1208-1222, 1329-1331, 1352

CONTENTS

PHYSICS

UDC: 621.383

DIGITAL DATA PROCESSING WITH OPTOELECTRONIC DEVICES

Moscow KVANTOVAYA ELEKTRONIKA in Russian Vol 6 No 6, Jun 79 pp 1125-1147

[Article by E. A. Mnatsakanyan, V. N. Morozov, and Yu. M. Popov]

[Text] This article contains a review of literature on optoelectronic methods of digital data processing. The authors examine the possibilities of designing various optoelectronic logic elements and arithmetic units based on these elements. The authors analyze processing methods in optical memory systems and design features of optoelectronic computing devices operating in nonpositional notation systems and redundant systems. The authors present the principles, as described in the literature, of design of optoelectronic processors operating with two-dimensional data files. The authors appraise their potential and the capability of optoelectronic computing systems to compete with electronic computers.

Introduction

At the present time development of computer hardware is determining in large measure advances in various fields of science and technology. Therefore it is entirely logical that close attention is being focused on presently-existing computer systems based on traditional electronic components, their development and improvement, as well as the development of new elements and principles of designing computers.

The development of computers based on large integrated circuits (LIC) was a major step toward solving the problem of high-output information processing. It made it possible sharply to reduce the physical size of computers, power requirements, and equipment unit cost. Nevertheless further increase in computer speed remains a current problem, since electronic computing devices possess certain fundamental deficiencies which impede progress in this area [1].

Consequently we must seek new principles of designing computer systems. One possible way is the utilization of optoelectronic computing devices.

Advances in optics are making it possible to reapproach the problem of designing high-output computer systems. This approach is based on the idea of

utilizing a light flux as information carrying medium. To implement this idea we must develop methods of acting upon a light flux, essential for performing various logical and arithmetic operations, and frequently fairly complex calculations as well. Interest in optical methods of processing information is due to a number of new capabilities not possessed by the traditional electronic processing methods:

extensive employment of parallelism at different levels;

better decoupling between input and output as well as between transmission channels in comparison with electronic computers;

utilization of picture logic, which makes it possible to develop new principles of performance of operations which are not customary for electronic computers;

storage of binary or analog signals in holographic form;

a basic capability to process discrete and analog signals with one and the same components.

Considerable progress has been achieved in developing optical computer systems of an analog type, correlators and spatial filtration systems, for example. According to estimates by the authors of [2], the speed of processing and output of images for such systems, even with the number of elements at 1,000 x 1,000 with eight bits of luminance levels, reaches 600 Gbit/s for processing and 0.24 Gbit/s for speed of photoprinting finally-processed images, beginning with input. This is not only as a result of parallel processing but also a result of the "high speed" of optical lenses, which provide a considerably greater processing speed than digital methods. However, the inflexibility and poor accuracy of computations by optical analog devices means that they can be utilized only in specialized peripheral devices of electronic computers for preliminary image processing.

Utilization of optical methods for discrete information processing is a more complex problem. This is connected both with the high level of development of digital electronic computer hardware and insufficient attention directed by investigators to the problem of optical digital computing equipment and its component base.

Nevertheless certain devices employing optical methods and components have already been developed and are being utilized. In the IBM-3666 computer, for example, a laser is employed as an element for reading product code and in the IBM-3800 -- for exposing electrographic structures at a rate of 13,360 lines per minute in document printing; a small-capacity permanent holographic memory (PHM) is also being utilized, and the Unicon optical memory has been developed, based on burning holes in a tape with a density of 4×10^6 bit/cm^2, the "Laser-Photo" system, etc [3, 4].

Development of optical methods of information processing, improvement of sources of radiation (coherent and noncoherent), as well as development of

APPROVED FOR RELEASE: 2007/02/08: CIA-RDP82-00850R000100090042-5

optically controlled transparencies (OCT) and reversing media make it possible closely to approach development not only of individual components of digital information and computer systems but also entire processors. Several directions have been noted up to the present time in solving this problem. Some of them call for practically complete copying of electronic systems, with replacement of each electronic component with a corresponding optical component, while others call for totally different methods of building such systems. In our opinion, in view of the considerable advances in development of traditional electronic computers, only fullest utilization of the above-specified features of optical information processing alongside improvement of the component base will enable the optical processor not only to compete with the electronic computer but also in a number of instances to solve problems which electronics cannot handle.

In this article we have endeavored to examine the principal directions of research in the area of development of digital optical processors, the development prospects of this research, and to assess the possibilities of the various proposed systems.

1. Optoelectronic Elements and Arithmetic Units Based on Them.

1. Optoelectronic logic with semiconductor lasers. Study [5] was one of the first research projects aimed at development of optoelectronic logic elements based on a semiconductor laser-photodiode system. The authors performed theoretical and experimental investigation of the characteristics of such a system, for the purpose of utilizing it to develop computer devices, the structure and principles of organization of which would be identical to traditional devices based on electronic components. It is essential thereby to take into consideration the requirement of completeness of the set of logical operations [6]. Factors involved in selecting such a system include low inertia (to 10^{-10} s), high laser efficiency, as well as high photodiode sensitivity and speed.

The first components to be developed operate at the temperature of liquid nitrogen, which was a hindrance to their practical application. Quite recently, however, there has been an increase in interest in such components in connection with the development of integral optics and improvement in the characteristics of injection lasers (continuous operating mode at $T=300^{\circ}$ K, with a service life of several tens of thousands of hours, and pumping currents have been reduced to tens of milliamps [7, 8]).

Employing logic elements based on a laser-photodiode, one can produce a functional diagram which performs various operations. It is reported, for example, that a three-element integrated circuit has been developed: an injection laser, a plane passive lightguide, and a photodetector [9]. All elements are shaped by processing blanks through common masks and subsequent selective etching. The device operated in quasi-continuous mode at room temperature. The process also made it possible to place on a single crystal a circuit with a larger number of radiators and photodetectors with controlled optical links between them. Such an approach, however,

contains serious shortcomings [3]. In particular, in any logic element where there is a dual electricity-light-electricity conversion consumed power is appreciably greater than with electronic devices, and it is difficult to produce a circuit with a large number ($\gtrsim 10^3$) of elements and links between them. Therefore extensive employment of such logic elements as principal elements in computer hardware is questionable; more probable is their employment in terminal devices of optical communication links, as decouplings, etc.

2. Planar and waveguide optical logic elements. Recently studies have been published dealing with the development of planar and waveguide optical logic elements and switches.

A planar device [10] constitutes a multilayer structure with a photoconductor, with specially shaped electrodes applied on the structure's electrooptical layer. The structure is placed between polaroids. Light striking the photoconductor changes its resistance and, consequently, phase delay on the electrooptical crystal. Varying the shape of the electrodes and the mutual orientation of the polaroids, one can perform logical operations comprising as an aggregate a complete system of Boolean algebra functions. If we assume that the described structure provides a resolution of 20 lines/mm in a field measuring 7.5 x 7.5 cm and the optical switching time is 100 microseconds, its output can be considered to exceed 10^9 bit/s. Planar devices, however, possess substantial efficiencies (external polaroids, shaped electrodes, etc).

Considerably more interesting are attempts to design logic and arithmetic units based on waveguide elements [11-14]. Such elements can arbitrarily be divided into two groups: interference waveguide modulators, and paired waveguide switches. The operating principle of interference waveguide modulators (Figure 1a) is based on division of the input beam into two branches, with electrical signals applied to each branch with the aid of electrodes. After the two branches are brought together into a single output waveguide, there will be an optical signal in it when the phase difference in the branches is

$$2\pi N \ (N=0, \pm 1, \pm 2, \pm \ldots).$$

Each electrode, when electrical signal V_0, with an amplitude of several volts, is applied to it, shifts the phase of the light passing through the corresponding branch by π. If the initial path difference in the two branches is π (this can be achieved by applying constant voltage V_0 to one of the electrodes), then, in relation to the presence of signals on the other electrodes, the appropriate set of logical operations can be performed.

Paired waveguide switches (Figure 1b) comprise two waveguides placed on a backing, with sections located at a distance of several wavelengths from one another. If the characteristics of these sections are identical, and there is light in one of the waveguides, luminous energy is transferred into the adjacent waveguide. When a signal is applied to one of the electrodes transfer does not occur, since the characteristics of the segments become different. Thus logical operations $(a \bullet b)$ and $(a \bullet b)$ are performed.

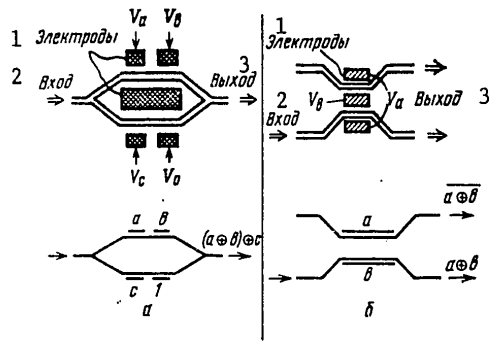

Figure 1. Waveguide Optical Logic Elements

Key:
1. Electrodes
2. Input
3. Output

In study [14] the switching time of such logic elements, due to the short length of the branches, is estimated at 20-40 ps, and scattered energy comprises ~30 pJ, that is, it is less than in electronic elements (50-100 pJ). Joining waveguide logic elements in this manner, one can perform a logic function of any type. In particular, both various logic circuits and the circuit of a 16-digit adder are examined in [14].

Paired waveguide switches can also be used as electronic deflectors in a waveguide arrangement, controlled by low-amplitude signals [10, 11]. They make it possible to switch the direction of propagation of a laser beam (up to 4-8 directions).

Waveguide circuits for logic devices and arithmetic units are more progressive than the others described above. Compactness, capability of connecting up with other circuits with the aid of lightguides, high speed, and little dissipated power make them highly attractive. However, difficulties in designing logic circuits with two-dimensional input and output make possibilities of information processing based on these circuits considerably less than with utilization, for example, of controlled transparencies (CT).

3. Logic element and arithmetic units based on space-time light modulators -- controlled transparencies. Studies [15-18] suggest principles of designing logic elements and arithmetic units based on CT and investigate the characteristics of such devices. Schematically a CT constitutes a discrete light-valve device which can be organized in the form of a matrix, each point of which corresponds to storage and processing initiation of one bit of information.

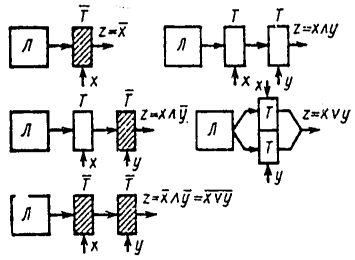

Figure 2. Obtaining Various Boolean Functions With the Aid of CT

Let us examine performance of the simplest logical operations with a CT. Figure 2 contains as an example diagrams showing certain logic functions. Here letter T designates CT which pass laser light ($\mathcal{U}$) in the presence of a control signal (x=1), and letter $\overline{T}$ -- in the absence of a signal (x=0). One can readily see that conjunction (logical multiplication) from n variables is realized with the aid of sequential laser beam transmission through n single-element CT, and disjunction (logical addition) -- by the joining (focusing) of the outputs of one n-element CT.

We know from Boolean algebra that any Boolean function can be represented in conjunctive and disjunctive normal form. Thus, utilizing the elementary logic circuits shown in Figure 2, we can realize any logic and arithmetic function of a finite set of binary variables.

As an illustration we shall examine the principles of design of a CT adder. When adding two numbers ($X=x_1x_2\ldots x_n$ and $Y=y_1y_2\ldots y_n$) the principal task consists in determining a third number $E=e_1e_2\ldots e_n$, the digits of which indicate the presence or absence of transfers to the corresponding digits of the logical sum. The true sum is

$$\Sigma = X \oplus Y \oplus E$$

(here and henceforth $\oplus$ -- symbol of digit-by-digit adding). As we know [6], e_k is calculated with the formula

$$e_k = \sum_{i=k+1}^{n} \bigcap_{j=k+1}^{i-1} x_i y_i t_j,$$

where Σ -- logical addition symbol; $\bigcap$ -- logical multiplication; $t_j = x_j \vee y_j$.

If e_k are determined, the true value of k digit of the sum can be obtained with the formula

$$\sigma_k = \overline{x}_k y_k \overline{e}_k \vee \overline{x}_k \overline{y}_k e_k \vee x_k \overline{y}_k \overline{e}_k \vee x_k y_k e_k.$$

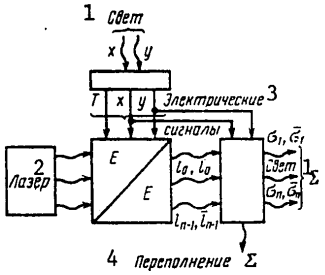

Figure 3. Diagram of Ultraparallel Adder

Key:
1. Light
2. Laser
3. Electrical signals
4. Overflow

Based on these formulas, one can design an adder utilizing methods of realization of Boolean expressions on CT. Figure 3 contains the diagram of an ultraparallel adder which does not contain a line of carries. Here unit E, consisting of n+1 CT, forms the signs of carries e_k, and unit Σ forms the final result. This adder is fairly fast (up to 20 MHz), with power requirements of 10 watts [17]. The ratio of energy at adder input to energy at output for one cell is determined by the formula

$$j = W_{\text{н}}/W_{\text{к}} = 1/\alpha^m,$$

where α -- coefficient of transparency of CT; m -- number of transparencies in adder.

For large m (for example, 64), even when $\alpha = 0.9$, attenuation j reaches $\sim 10^3$, which constitutes a substantial limitation of this device, alongside extremely high (in comparison with an electronic adder) power requirements.

More promising is an adder consisting of several byte adders connected by a chain of carries. If numbers contain 64 digits, it is advisable to employ eight byte adders, and although this reduces speed eightfold, a great simplicity of circuitry is obtained, with an overall decrease in power requirements. Other arithmetic units (AU) which are components of the processor are constructed in like manner. Evidently such an approach can be utilized for designing any individual arithmetic unit, while it is inadvisable to design a processor as a whole on this basis.

4. Optoelectronic devices operating in a system of remainder classes (SRC) and in positional notation systems with redundancy. In order to avoid difficulties connected with performing carries for purposes of the arithmetic, it was proposed to work in nonpositional notation systems, in particular in systems of remainder classes [18, 19, 21]. As we know [20], there

are no links between individual digit places in such systems; each digit is processed individually, and the result can be obtained immediately in all digit places, which makes the operations of addition, subtraction and multiplication single-step.

For the sake of simplicity we shall examine here the processing of positive integers; utilization of negative numbers and non-integers in SRC is discussed in detail in [20]. As we know [20], whole numbers in SRC are represented in the form of least positive remainders from the division of these these numbers by mutually simple bases

$$\rho_1, \rho_2, \ \dots\ , \rho_{n-1}, \rho_n,$$

called moduli:

$$A=(\alpha_1, \alpha_2, \ \dots\ , \alpha_n)=k_1\rho_1+\alpha_1= \ \dots\ =k_i\rho_i+\alpha_i = \ \dots\ =k_n\rho_n+\alpha_n,$$

where α_i -- least remainder from dividing A by ρ_i; k_i -- integers. Obviously the range of representation of numbers is limited by the product of moduli $M=\prod_{i=1}^{n}\rho_i$. Usually M lies within limits 10^{10}-10^{16}, while since in electronic arithmetic units as a rule prime numbers from 2 to 61 are selected as bases ρ_i, 15-18 bases are needed, the number of which increases with an increase in M.

Let us examine as an illustration an arithmetic summation of the numbers 87 and 49, represented in the SRC by radices 5, 7 and 9:

$$\begin{array}{rr} 87 \rightarrow & 236 \\ +49 \rightarrow & +404 \\ \hline 136 \leftarrow & 131 \\ 136 \leftarrow & 131 \end{array}$$

In this example 87 is converted in the SRC into (2, 3, 6), where 2 is the least remainder from dividing 87 by 5; 3 -- from dividing 87 by 7; 6 -- from dividing 87 by 9. The second summand, 49, is transformed in like manner. Each column is added independently and the result is presented as the remainder on the corresponding radix (modulus). For example, in the first column 2+4=6, but this is 1 on modulus 5. The result (1, 3, 1) signifies that the actual result when dividing by 5 has a remainder 1, by 7 -- remainder 3, by 9 -- remainder 1. Each column can be processed by different methods, tabular, for example (see below). Other operations are performed in the SRC in like manner.

These operations can be divided into modular and nonmodular, by degree of difficulty. Modular operations include the operations of addition, subtraction, multiplication, etc, and nonmodular -- division of numbers, comparison, determination of range overflow, etc. Modular operations are easily performed, while performance of nonmodular operations presents considerable complexity. A decrease in the magnitude of radices with a simultaneous increase in their number simplifies the circuitry of digit processors, but the time to perform nonmodular operations increases significantly thereby, since they are performed in sequence on all radices.

In optoelectronics, utilizing a tabular method of processing in SRC, larger radices can be selected than in electronic devices. The authors of [18] state that it is expedient to employ radices somewhat smaller than 2^K, where K=8-10. The table of results contains from 2^{16} to 2^{20} addresses thereby. Representation in an SRC of numbers 10^{10}-10^{16} in magnitude when K=8 requires 5-7 radices, that is, their number is reduced, and consequently nonmodular operations are performed more rapidly. Nevertheless it is impossible fully to eliminate the difficulties mentioned above.

One attempt to avoid these difficulties is the designing of a combined processor in which modular operations are performed in an SRC, and nonmodular in a positional notation system. One can utilize the positive qualities of both systems in such an optoelectronic processor and eliminate to a significant degree the deficiencies individually inherent in each. However, it is advantageous to build combined units only under the condition of rapid transfer from one system of notation to the other and back.

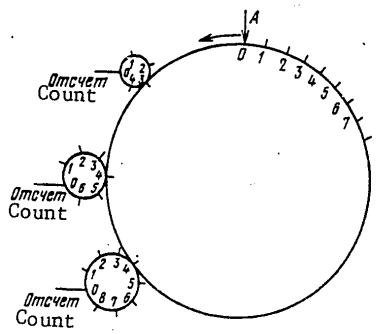

Figure 4. Basic Diagram of Changeover of Numbers from a Positional System to an SRC

Of particular interest from this standpoint is [22], in which the author has elaborated the principles of changeover from an SRC to a positional system and back with the employment of optical methods. The idea of changeover from a positional system to an SRC consists in the following. Remainders on each radix possess the property of cyclicity, that is, repeat following a period equal to the radix. Therefore, by breaking each period down into a number of identical intervals equal to the value of the radix, one can change over number n into an SRC, proceeding on a cycle of n steps. Figure 4 illustrates this. Marked out on large circle A are numbers in a positional system (decimal, for example), while the small circles are divided into p_i parts (p_i -- selected moduli in the SRC). If all disks are initially set to zero, then by selecting number n on A, we obtain the values of the remainders of this number by moduli on the corresponding disks. In optics this can be achieved on the basis of rotation of the plane of polarization of a beam or change in the phase of a light wave. It is clear that this

conversion is sequential (step by step), but simultaneous for all moduli. However, there exist methods of significantly reducing the conversion time by utilizing such a method [22].

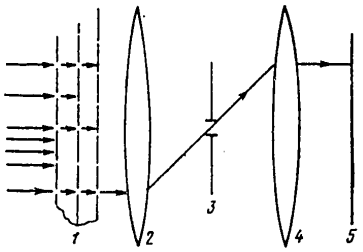

Figure 5. Diagram of Parallel Conversion of Numbers From an SRC to a Positional Notation System

Key:

1. Set of grids
2. Lens
3. Aperture
4. Lens
5. Scale graduated in the corresponding positional system

Figure 5 contains an optical arrangement for converting numbers from an SRC to a positional system. The principal elements of this arrangement are grids in which distances between apertures are proportional to moduli (in this case 5, 7, and 9). The digits of the number represented in the SRC indicate how much the grids are displaced relative to zero level, that is, a case where all remainders are equal to zero, and the grid beginning points coincide. Obviously the light beam to the right of the grids will be only at that level where the apertures of all three grids coincide. The beam then passes through a confocal system of lenses. At the common focal point there is a diaphragm which arrests all scattered light other than the beam. After passing through the entire optical system and striking a scale graduated in a positional system of notation, the light beam strikes a point corresponding to the number sought. Since mechanical displacement of the grids is not practical, the author of [22] suggests displacing the light beam relative to the grids, utilizing Kerr cells or other optical shifting devices. Obviously such a method of conversion is parallel, and therefore conversion time is minimal. The limitations of this method are evidently due to the finite apertures of the optical elements utilized and their speed.

The authors of [23] examine the design of an arithmetic unit which performs ddition and multiplication in an SRC. Following are the principal components of this device: an electronic interpreter, which converts operators from a positional system to an SRC light-emitting diodes, the radiation of which controls the OUT [space-time light modulators]; a phase OUT with a linear characteristic curve; a counting laser; a matrix of photodiodes and an electronic interpreter which performs inverse transformation. The authors of this project, timetabled for 1980-1985, hope to achieve a speed of 5×10^{11}

addition operations per second, although there exist a number of serious difficulties which must be surmounted in the course of the project.

Also of definite interest is employment in optoelectronics of positional systems with redundancy of representation, since as a consequence of this carries forming as a result of computations extend not beyond one (adjacent) digit place. The authors of [24] propose an adder of two arrays of numbers, utilizing a positional system of notation with dual redundancy. Each digit in such a system is recorded by two symbols (half-digits), as a consequence of which it is called a system of notation with half-digits (SHD). An SHD with a radix of 2 retains the polynomial form of binary number notation, but each digit consists of two parts: $h_i=(\beta_i 2^1+\alpha_i 2^0)$, that is, each digit place can contain the following digits: zero -- 00, one -- 01, two -- 10, three -- 11. The normal form of notation of a binary digit is "single valued" (with zero value of the high-order half-digit), while only the low-order half-digit is inverted in each digit when forming the complement and reciprocal.

Following is the algorithm for adding the numbers a and b in an SHD [25]:

$$c'=(a \oplus b) \vee (a \cdot b)_{\leftarrow 1/2},$$

where $a \oplus b$ -- bit-by-bit sum; $(a \cdot b)_{\leftarrow 1/2}$ -- result of logical multiplication of numbers with subsequent left-shift by one half-digit.

In connection with the redundancy of SHD, number notation may not appear in normal form as a result of addition. The number 2, instead of (0100) may be represented as (10), and the number 3 -- as (11) (in place of (0101)). This makes it impossible to add more than two sets, since combinations of the type (10) nad (11), obtained as a result of adding two numbers, should be reduced to the normal form C prior to the subsequent arithmetic operation. The operating principle of a device for eliminating ambiguity [26] is based on the transformation of K-digit groups of digits into which the number is broken down, into normal form with the aid of finding their unambiguous equivalents in the memory unit.

The speed of performance of addition in such an adder is limited by the speed of the transparencies. Theoretically the rate of finding c' may exceed 10^9 operations per second for 32-digit numbers with transparencies measuring 128 x 128, but this figure diminishes significantly in case of the necessity of normalization of result c'. Another shortcoming of this device is utilization of the interference principle of interaction between two light beams, since this imposes rigid limitations on the optical elements, alignment and circuit operating conditions.

The author of [27, 28] has developed a theory of notation called sign-digit representation (SDR). SDR are positional redundancy systems in which each digit of a number is represented by a digit with sign. The radix can be any positive integer exceeding 2 ($r \geq 3$). While with the customary representation of numbers in systems of notation with a whole-number radix ($r > 1$) each digit can accept only r values: 0, 1, 2... (r-1), in an SDR each digit can assume q values in conformity with the relation $r+2 \leq q \leq 2r-1$. Both positive and

negative digits are used in SDR, while the number of utilized digits is greater than in conventional positional systems. Thus an SDR has redundancy, due to which each digit place in a sum or difference is a function of the digits positioned only in two adjacent digit positions of each number participating in the operation. Therefore in an SDR one can perform entirely parallel addition and subtraction.

The above-discussed systems of notation and computer devices based on these systems make it possible to utilize with great effectiveness the capabilities of parallel processing in optoelectronics, and in our opinion the capabilities of these systems are far from exhausted. Therefore further research is needed, directed toward utilization of various systems of notation in optical processing of information.

II. Digital Processing in Memory Systems

1. Tabular method of processing information in optical addressed memories. The idea of using memories for performing logical, arithmetic operations and combining the functions of information storage with the function of information processing has been studied fairly intensively [29-33]. One of the first proposals was an attempt to utilize addressed holographic memories (HM) for designing tabular-type arithmetic units and processors based on these units. The tabular method consists essentially in the fact that tables are placed in memory, tables corresponding to the values of various functions, while the process of computation consists in finding the table values of a function by address-argument. In some electronic computers (for example, the IBM-1620, ICT-1500) [34], tables are stored in main memory, but their small volume permits processing only numbers of very small wordlength (3-4 binary digits).

Evaluations of HM storage for tabular arithmetic lead to the following results. Any operation can be represented in the form $Y_i=f_e(x'_j, x''_k)$, where x'_j is the j value of the first operand x'; x''_k is the k value of the second operand x''; Y_i is the i value of the operation result (i operation). If we assume that the word length of the operands and all results represented by binary code is equal to m, total memory volume required for realization of a system of L operations can be determined from the equality

$$C=Lm2^{2m}.$$

For modern general-purpose electronic computers $L \geq 100$, and $m \geq 32$. If such a system of commands is realized with the aid of a tabular method, it will require a memory volume of $C=100 \cdot 32 \cdot 2^{64} \approx 10^{23}$ bits.

It follows from this that it is difficult to accomplish the task of designing a tabular processor with a sufficiently developed system of commands and required operand formats. Employment of tabular processors, which operate with small-format operands (for example, one-byte), requires the development of tabular-algorithm methods of data processing, which reduce to a sequential-parallel mode of performing operations. Therefore problems of developing

methods and techniques of reducing memory size without loss of precision and substantial decrease in speed are of considerable significance.

For example, employment of the tabular method in an SRC makes it possible substantially to reduce HM capacity. As was indicated above, each remainder in an SRC is processed independently, while it is advisable to select the bit configuration of the remainder ≈ 8. Substituting these values in the expression for C when L=100, we obtain $C=100 \cdot 8 \cdot 2^{16} \approx 10^8$ bits, which is an attainable capacity.

The tabular method can be implemented in a hybrid computer structure [35], which links GPZU [holographic permanent memory] for storing tabular values and an electronic computer for interpolation of results. Function j (x) is entered into memory, specified in the form of a table and interpolation coefficients which make it possible to determine the values of a function for the values of arguments which are located between adjacent table values.

2. Digital processing in optical associative memory systems. As we know [36], in associative memories information search is performed on the basis of description of the information -- features, key words. The authors of [29, 30] discuss the principles of designing optical associative memories utilizing holograms as information storage devices; they investigated the possibilities of performing simple search operations based on computation of a system of simplest logic functions. Further development of such HM is reported in [33, 37, 38], which describe a functional model of an associative optical HM with a two-level organization of memory and questions of hardware realization of functions utilized for complex information search.

The first, basic memory level is intended for storage and addressed retrieval of data files, while the second, feature level is intended for storage of descriptions of these files and direct-access address search at user request. Search is performed by comparing the inquiry word with the content of the feature memory storage locations.

Let files of digital, alphanumeric, graphic and other data (D_1, ..., D_h ..., D_H) be stored at the main memory level. The files are stored at locations the addresses of which are unambiguously linked to their numbers (1..., h, ... H). Corresponding to each of the files D_h in the feature memory is a description comprising a set of R key words

$$K_h = \{k_{h1}, \dots, k_{hr}, \dots, k_{hR}\}, \quad \text{where} \quad k_{hr} = (k_{hr1} \dots k_{hrN}) \quad --$$

N-digit numbers. We enter an inquiry in similar fashion:

$$Z = \{z_1, \dots, z_r, \dots, z_R\}, \quad \text{where} \quad z_r = (z_{r1} \dots z_{rN}) \quad -- \text{ a binary}$$

number also containing N digits. Equality of numbers of digits in key words and inquiry words is adopted for simplicity.

Accessing of information from memory is performed in two stages. At the first stage the value of a homogeneous system of H logic functions

$$Y_r=\begin{bmatrix} \overline{y_{1r}} \\ \dots \\ y_{hr} \\ \dots \\ \overline{y_{Hr}} \end{bmatrix}.$$

is computed in characteristic or feature memory for each of R inquiry features. The addresses of the data files corresponding to the search result on the set of attributes or features are computed in feature memory by forming file

$$A=(a_1,\ a_2,\ \dots,\ a_h,\ \dots,\ a_H), \quad \text{where} \quad a_h=\bigcap_{r=1}^{R} y_{hr}.$$

The sought information is retrieved from principal memory at the second stage of search on the basis of the obtained addresses.

The problem of information search by type of systems of functions Y_r can be divided into two groups. The first group includes problems of retrieving files the key words of which are equal (not equal), more (less), not less (not more), and also are logically linked with corresponding key words in the inquiry or lie within specified boundaries. For this group of retrieval problems it is necessary to compute a system of logic functions of the type

$$y_{hr}=f(z_r,\ k_{hr}),\ h=1,\ 2,\ \dots,\ H. \qquad (1)$$

This signifies that for each h memory address a specified logical relationship between the digits of like key words of description of h file and inquiry is realized.

It follows from [37] that system of functions (1) can be presented in disjunctive form

$$y_{hr}=\bigcup_{q=1}^{Q} \overline{P}_{hrq},$$

where $P_{hrq}=\bigcup_{n=1}^{N}(z_{rnq}\bar{k}_{hrn}+\bar{z}_{rnq}V_{hrn})$ -- function of non-equivalence between key words k_{hr} and inquiry words z_{rq}; $\bigcup$ -- logical sum symbol; Q determines the number of iterations needed to compute function y_{hr}, while inquiry word z_{rq}, in contrast to inquiry word z_r, depends on the step number. $z_{rq}=\varphi(z_r)$ where φ is determined by the retrieval task being performed. The number of digits in z_{rq} is also equal to N, with the difference that these binary digits, other than the values 1 and 0, can assume a neutral state designated by the symbol M (mask), and not take part in the computation.

For example, if one wishes to find the address of files the key words of which are equal to like inquiry key words, in this case Q=1, $z_{rq}=z_r$. In solving more complex problems Q differs from 1.

A second group includes problems of retrieving data arrays the key words of which are extremal (among the specified set of descriptions), the closest larger (smaller) to the inquiry word and ordered in magnitude. A system of logic functions of the following type is calculated in solving such problems:

$$y_{hr}=(z_r,\ k_{hr},\ k_{sr}),\quad h=1,\ 2,\ \ldots,\ H. \qquad (2)$$

In contrast to expression (1), these logic functions are determined not only by the digits of the inquiry key words z_r and corresponding description address k_{hr} but also by the digits of the key words of the descriptions of other arrays: k_{sr}; s=1, 2, ..., H; $s \neq h$.

The authors of [37] present in detail algorithms for calculating functions y_{hr} of the first and second groups of inquiry problems, and in our opinion it is advisable here to discuss only the conclusions and results of this study.

The task of data array address search is performed by systems of the computer-external storage type. External storage units perform the functions of information storage and output, while the computer performs the functions of information processing. Retrieval time is determined by the time to transmit data through the external storage unit-computer communication channel and the time required for inquiry processing by the program. The output of such a system can be substantially increased if the addresses of the data arrrays are calculated directly in memory by hardware means. Some operations (non-equivalence functions, for example) on inquiry key words and data array descriptions are performed in the optical channel of the HM, while performance of operations not characteristic of optical systems is handled by the HM photoelectronic system which, in contrast to the photomatrix of the conventional HM, should be supplemented with electronics, making it possible to perform logical data processing.

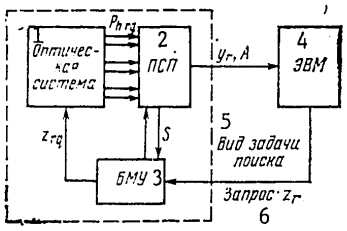

Figure 6. Diagram of Retrieval System

Key:
1. Optical system
2. PPP
3. MCU
4. Computer
5. Type of retrieval task
6. Inquiry

Figure 6 contains a diagram of a retrieval system of this type. Employed here is a feature or characteristic HM, which includes an optical system, a parallel page processor (PPP), and a microprogram control unit (MCU). The type of retrieval task and inquiry word z_r are specified by the computer. The MCU forms the optical system inquiry words and controls operation of the PPP in conformity with the retrieval task to be performed. Only the desired address array A is transmitted to the computer in this case through the HM-computer channel. With this organization of the HM, data array access time can be reduced by two to three orders of magnitude.

A key word search correlation mechanism is an attractive basis for designing optical associative memories, since it becomes possible to search for a single word or simultaneously to search for several key words through the entire memory, independent of the order of placement of words within each location. The autocorrelation functions of the key words should be close to δ functions, while mutual correlation functions should assume minimum values.

They author of [39] draws the conclusion that it is convenient to utilize binary orthogonal sequences for optical data processing methods. Reid-Mueller codes are the basis for their design. This design of an associative optical memory also makes it possible to perform various types of search (that is, "greater than" and "less than" operations, extremum search, etc), but the data arrays should be arranged on the basis of some parameter.

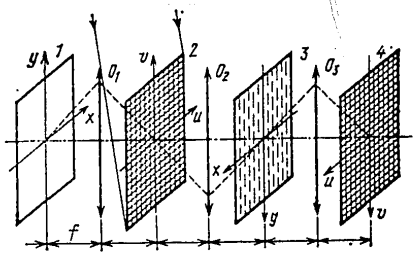

Figure 7. General Diagram of an Optical System of an HM with Information Processing Functions

3. Transformations performed in optical systems of HM with matrix memory organization. Let us examine a general diagram of such an HM with data processing functions (Figure 7). Here 1 is the plane of the recorded image; 2 -- hologram matrix plane, which is struck by a plane wave; 3 -- restored image plane; 4 -- output frequency plane. Planes 1 and 3, 2 and 4 are projectionally linked by objective lenses O_1 and O_2, O_2 and O_3. Planes 1 and 2, 2 and 3, 3 and 4 are interconnected by a Fourier transform effected with the aid of objective lenses O_1, O_2, O_3. The coordinates in planes 1 and 3 are designated by symbols x, y, and in planes 2, 4 -- η, ξ. Angular spatial frequencies u and v in planes 2 and 4 are linked with linear coordinates ξ and η by relations

$$u=2\pi\xi/(\lambda f),\ v=2\pi\eta/(\lambda f),$$

where f -- focal length of the lenses effecting the Fourier transform; λ -- wavelength of light. If we assume that the region of the task of function (f_{mn} (x, y) -- representation of a page of information stored in a hologram -- is Ω, the distribution of intensity of light in plane (u, v) will be described by the expression

$$J_r(u,v) = \int_{-L_B/2}^{L_B/2}\int K(x,y,u,v)\,dxdy,$$

and in plane (x, y)

$$J_B(x,y) = \int_{-L_r/2}^{L_r/2}\int K(x,y,u,v)\,dudv,$$

where L_B -- linear dimension of the restored image; L_r -- angular dimension of the hologram matrix; K (x, y, u, v) -- a certain kernel determined by function f (x, y) (by the content of the hologram matrix).

If we place in plane 3 a transparency with amplitude transmission $\varphi^{1/2}$ (x, y), distribution of intensity in frequency plane 4, equivalent to hologram plane 2, will be described by the expression

$$I_r(u,v) = \int_{-L_B/2}^{L_B/2}\int \varphi(x,y)\,K(x,y,u,v)\,dxdy. \qquad (3)$$

In like manner, if a transparency with amplitude transmission $\varphi^{1/2}$ (u, v) is positioned in the plane of hologram matrix 2, then in plane 3 intensity will be distributed according to the law

$$I_B(x,y) = \int_{-L_r/2}^{L_r/2}\int \varphi(u,v)\,K(x,y,u,v)\,dudv. \qquad (4)$$

Expressions (3) and (4) comprise a pair of linear two-dimensional integral transformations with a kernel of a general type. Kernel K (x, y, u, v) is determined by the content of the hologram matrix and is actual and normalized. Forming of the kernel takes place by recording in each Fourier-hologram with coordinates u_m, v_n images distribution of the intensity of which is proportional to $K(x, y)\big|_{u=u_m,\ v=v_n}$. Corresponding to each point $x=x_k$, $y=y_1$ in the plane of the restored image is distribution of intensity in the plane of the hologram matrix $K(u, v)\big|_{x=x_k,\ y=y_1}$.

Due to the finite dimensions of the holograms and consequently the spatial discretization of the processed images in HM optical systems, what is actually realized is not integral transformations (3), (4), but their discrete analogs, which are convenient to represent in matrix form. One can easily see that transformation (3) is equivalent to multiplying rectangular matrix by matrix-column, and transformation (4) -- multiplication of matrix-line by rectangular matrix.

The class of transformations effected in HM optical systems can be expanded by changing the angle of incidence of the restored beam onto the hologram. In this case, when restoring the hologram matrix with light waves with differing phase front inclination, one can perform simultaneous processing of several images. An expression corresponding to this case is equivalent to a matrix equation,

$$\| a_{jp} \| = \| k_{ji} \| \times \| \varphi_{ip} \|, \qquad (5)$$

where $a_{jp} = \sum_{i=1}^{I} k_{ji}\varphi_{ip}$ -- result of transformation of one of P images;

$\| a_{jp} \|$, $\| k_{ji} \|$, $\| \varphi_{ip} \|$ -- rectagular matrices.

The size of the matrices in expression (5) is determined by the allowable change in angle of incidence ε of the restored light beam on the hologram matrix. With multiplication of square matrices $J=I=P=(\varepsilon l_г/\lambda)^{2/3}$, where 1 is the linear dimension of the side of a hologram matrix. One can demonstrate that taking into consideration the limitations caused by deformation of the restored image and decrease in its luminance, allowable change in angle $\varepsilon \approx \pm 2°$. If $l_г = 100$ mm, $\lambda = 0.63 \times 10^{-3}$ mm, then under the conditions of multiplication of square matrices, their size is equal to $J \times I = I \times P = 4 \cdot 10^2 \times 4 \cdot 10^2$.

Since linear integral transformations with a difference kernel are realized in the HM system we are discussing, correlation functions can be computed right here, both sequentially and in parallel. In the first case a transparency positioned in plane 1 is sequentially illuminated by plane waves with a differing phase front inclination, while in the latter case a transparency with an image is illuminated by a set of plane waves. In addition, associative information search, spectral analysis of images on any basis, and other types of processing are effected in these HM systems. The transformation kernel can be changed with replacement of memory module in the case of a read-only HM or information rewrite in the case of a direct-access HM.

We should note that significant shortcomings of such systems are the capability of realization of only a narrow class of the above-indicated transformations with an unaltered HM structure and that the result of transformations is presented in analog form regardless of the type of information stored in the hologram matrix and information recorded on the transparency.

III. Optoelectronic Processors

1. Optoelectronic processor with variable operators. A fundamentally new approach to design of an optical processor was proposed in [40-42]. As we know, any computing process consists of a number of transformations of a set of input variables -- operands. Mathematically this can be represented in the following form:

$$X_2(\eta, \xi)=\hat{\varphi}_1 X_1(\eta, \xi),$$
$$X_i(\eta, \xi)=\hat{\varphi}_{i-1} X_{i-1}(\eta, \xi),$$
$$X_n(\eta, \xi)=\hat{\varphi}_{n-1} X_{n-1}(\eta, \xi), \quad Y=X_n(\eta, \xi),$$

where X_i -- input variables in i cycle and output variables in (i-1) cycle, specified in two-dimensional form (stages); $\hat{\varphi}_i$ -- i operator corresponding to the given base operation (that is, an operation performed by the hardware); Y -- result of the entire computation, consisting of n sequential base operations.

The proposed principle is based on storage in the computer memory not of operation results, as in a tabular processor, but rather operators $\hat{\varphi}$. This proves possible since corresponding to a logical or arithmetic operation is a certain operator or set of operators $\hat{\varphi}$, which depends only on the type of operation and is independent of input variables, whereby operator $\hat{\varphi}$ also comprises a discrete two-dimensional image. Consequently, the task consists in organization of an information processing circuit where it would be possible to realize the action of operators on input variables.

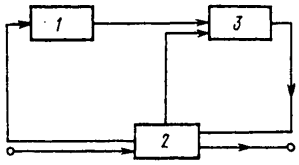

Figure 8. Diagram of an Optical Processor

Figure 8 contains a diagram of a possible optical processor variant containing such a circuit. Operators $\hat{\varphi}$ are stored in memory unit 1, storage unit 2 is the main memory, while information processing takes place in block 3. The processor works as follows: the file of input variables stored in 2 is projected onto 3, and operators $\hat{\varphi}$ are also projected onto it from 1. Corresponding processing of variables takes place in block 3, due to superposition of a page of variables onto a page of operators, whereby both discrete and analog signals can be processed. The result is read from 3, is rerecorded in 2, and then can serve either for further computations or for output onto peripheral devices. We shall note that block 3 can be based on space-time light modulators -- OCT.

Digital processing of information can be performed on the basis of the following equalities:

$$y_{ij}=\begin{cases} 0, & \text{if } z_{ij} \cap x_i = R, \\ 1, & \text{if } z_{ij} \cap x_i \neq R, \end{cases} \tag{6}$$

$$y_{ij}=\begin{cases} 1, & \text{if } z_{ij} \cap x_i = R, \\ 0, & \text{if } z_{ij} \cap x_i \neq R, \end{cases} \tag{7}$$

where R is a set which assumes values 0, 1 and $\emptyset$ ($\emptyset$ -- empty set).

Control of input signals is also possible on the basis of realization of equalities

$$y_{ij} = \begin{cases} 0, & \text{if} \quad z_{ij} \cup x_i = P, \\ 1, & \text{if} \quad z_{ij} \cup x_i \neq P, \end{cases} \tag{8}$$

$$y_{ij} = \begin{cases} 1, & \text{if} \quad z_{ij} \cup x_i = P, \\ 0, & \text{if} \quad z_{ij} \cup x_i \neq P, \end{cases} \tag{9}$$

where $\cup$ -- is a symbol signifying the uniting of signals z_{ij} and x_i; P is a set assuming values 0, 1 and 01. In (6)-(9) it is assumed that

$$Y = \{y_{ij}\}; \quad \hat{\varphi} = \{z_{ij}\}; \quad X = \{x_i\}.$$

Any of definitions (6)-(9) of the action of operator $\hat{\varphi}$ can be taken as a basis for designing an optical processor. Choice is determined by the specific type of CT employed. Essentially this method is positional, since the result is determined by the mutual positioning of discrete units in images $\{z_{ij}\}$ and $\{x_i\}$. We shall note that if z_{ij} and x_i are viewed as input variables, relations (6)-(9) are equivalent to the following logic functions: equivalence, nonequivalence, Scheffer stroke, etc. Obviously a CT carrying out the operation of inversion is also essential in some cases for completeness of realized Boolean functions.

As an example we shall examine the method of performing transformation (6) with the aid of a CT in which information is recorded and read at different wavelengths [43]. If control matrix $\{z_{ij}\}$ is projected at wavelength λ_1, while in reading the transparency is illuminated with variables $\{x_i\}$ at λ_2, at output the signal will be only at those points where x_i coincides z_{ij}. Figure 9 shows as an illustration transformation (8) of input variable $X=101$ by matrix

$$\{z_{ij}\} = \left\| \begin{matrix} 0\,1\,1\,0\,0 \\ 1\,0\,1\,0\,0 \\ 0\,1\,0\,0\,1 \end{matrix} \right\|.$$

Here variables and operators are represented in a paraphase code; an unshaded square designates the presence of light, and a shaded square -- the absence of light. Reflected light will occur only in those squares struck by light from both sides. We should note that one can also employ a transparency operating on transmission.

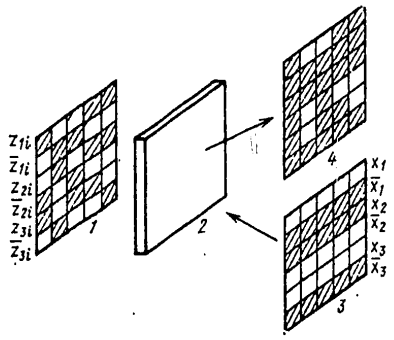

Figure 9. Transformation of Variable X=101 by Controlling Signal Matrix $\{z_{ij}\}$

Key:
1. Control signal $\{z_{ij}\}$
2. Optical CT operating on reflection
3. Input variables $\{x_i\}$
4. Result of conversion

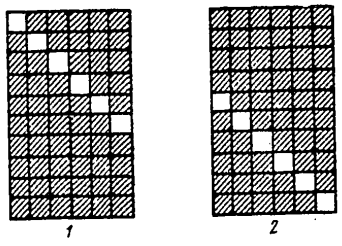

Figure 10. Type of Operator Fields for Shifting Numbers Two Positions to the Right

Key:
1. Operator field applied to control surface of first transparency
2. Operator field applied to control surface of second transparency

As an illustration we shall show how 3-digit number $A=a_1a_2a_3$ is shifted two positions to the right. The shift must be performed on two transparencies. Figure 10 shows the form of the operators which are applied to transparencies from storage unit 1 (see Figure 8). Input variables are applied to the first transparency in the form of horizontal bands of light. A signal will be reflected only from those squares struck both by light from the operator and from the input variables. Reflected light is expanded into a column and is applied to the following transparency in the form of vertical bands.

The operator projected onto this transparency modulates the light bands, and at output (in the light reflected from a second transparency) we have the number $B=b_1b_2b_3b_4b_5$ and equal to number A shifted two positions to the right.

One can easily see from Figure 10 and the above that a shift of any number of positions can be performed; this requires only appropriately changing the operator applied to the second transparency. We should emphasize that all logical operations in this optoelectronic processor are performed in a single cycle, that is, in one accessing to memory block 1.

Let us examine the functional capabilities of the proposed optical processor. Its principal difference from electronic computers is the absence of specialized units and circuitry performing various logical and other computing operations. It has only a common information processing circuit in which is performed parallel processing of a page with a capacity of 10^3-10^5 bits. Let us estimate the number of operators stored in memory block 1. Since capacity of an HM is approximately 10^8 bits, and each operator contains 10^4 bits, it is obvious that the number of operators can reach 10^4. This signifies that the given processor has the capability of paralleling not only by operands but also by commands (operations), and at the lowest level -- logic.

Since the processed page contains 10^4 bits of information, the number of different images totals 2^{10^4}. However, when employing a read-only HM as memory block 1, only 10^4 images (10^4 operators) are realized. This number can be increased by effecting 1 on a reversible medium. One can form new and change old base operators both independently and in the process of calculation, figuring in its results, that is, one can realize variable operators. All this has no analog in an electronic computer, and such a capability makes it possible easily to reorganize processor operation at the logical level, providing it with high output alongside paralleling.

Consequently such a processsor structure in our opinion makes it possible to perform various tasks with equally high efficiency as a consequence of the capability to utilize those computing methods which are most convenient for the given task. For example, the tabular method of computation, associative search, etc are easily performed.

Practical realization of such a processor is being held back primarily by the absence of or lack of perfection of an optoelectronic component base [42, 43]. In particular, development of digital CT of the linear (analog) type with utilization of electrooptical materials has encountered basic physical limitations, which impede achievement of the required speed and optical amplification. The following required CT parameters are cited in [44]: cycle frequency up to 10 mHz; numerical picture format $\sim 10^4$; luminance amplification (of 1 bit) greater than 20 decibals; power of reading source, up to 3 watts. One possible solution to this problem lies in employing a structure which combines an electrooptical layer with silicon integrated matrix of photosensitive control elements. The authors of [44] examine as

a universal integrated transparency cell a POMDME structure (photodetector-optical modulator-dynamic memory element), which constitutes a new microelectronic multifunctional device which combines the functions of a threshold photodetector and (or) a two-input AND logic element, a dynamic memory element, an injection-control switch, a capacitive voltage divider and an optical modulator of a reflecting type employing Pokkels longitudinal effect. The conclusion has been reached that integrated transparencies of all required types with a number of elements $\sim 10^4$ and the following parameters can be produced with these structures: OCT -- throughput $\sim 10^{10}$ bit/s with optical amplification of approximately 20 decibels and photosensitivity of 10^{-13} J/bit; electrical controlled transparency (ECT) -- optical channel input speed $\sim 10^9$ bit with an average light power of 10^{-5} watt per image element.

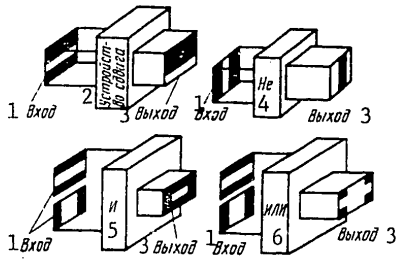

Figure 11. Explanation of the Basic Operating Principles of the Elements of Pictographic Systems

Key:
1. Input
2. Shift device
3. Output
4. NOT
5. AND
6. OR

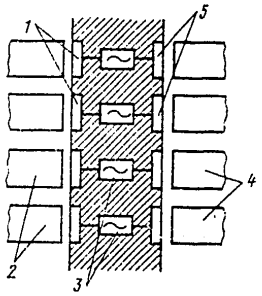

Figure 12. Schematic Representation of Negation Device

Key:
1. Photosensitive elements
2. Lightguides for information input and output
3. Electronic circuits performing inversion
5. Light-emitting elements

The projected output of an optoelectronic processor with variable operators employing transparencies with the specified parameters could correspond [43] to the output of an electronic computer with a speed of up to 10^{10} operations per second. Indeed, output can roughly be estimated with the formula V=KMf, where f is cycle frequency; M -- size of file to be processed; K -- coefficient of effective utilization of speed capability, which is determined by the class of problems being solved, machine structure, frequency of accessing peripheral devices, etc. Taking into consideration the above-named processor functional capabilities, one can hope to increase parameter KM by 10^2-10^4 times in comparison with an identical parameter in an electronic computer with f comparable to computer cycle frequency.

2. Hybrid devices utilizing picture processing. We shall define hybrid devices as those in which the bulk of operations are performed by specialized electronic devices analogous to corresponding electronic computer devices, while optics is used only for information transmission and simple processing.

One version of such a processor is proposed in [45]. Its component base consists of devices each of which performs a certain logical operation simultaneously for an entire discrete image. Figure 11 shows those units which perform the basic operations: negation, shift, AND operation, OR operation.

If we employ images containing N x N elements and perform logical operations on them simultaneously, then by designing a system which operates with images of 1024 x 1024 elements, we can achieve a speed of 10^2 times greater than electronic digital computers operating with 100-bit words, even if their speed is 100 times greater. Devices presently being developed contain 16,384 elements positioned in the form of a matrix of 128 x 128 elements 25.6 mm on the side. For these elements delay time is 5 milliseconds, but due to parallelism the effective processing speed is $3 \cdot 10^6$ bit/s.

Figure 12 shows schematically a device performing the operation of negation. An input image is applied through lightguides to photosensitive elements. These elements convert light signals into electrical signals, which in turn are inverted by electronic circuits. The inverter output signal is then applied to a light-emitting element. The inverter contains thin-film field-effect transistors as elements performing negation, and an array of electroluminescent elements for obtaining the output image. The other logic operations on the images are performed in analogous fashion, only electronic elements corresponding to other essential operations.

In order to design practically usable devices, pictographic (from picture) devices should be joined into more complex arrangements. In optical pictographic systems bunches of optical fibers are utilized to transmit images from one block to another. Although this simplifies realization of a large number of connections between elements and different circuits, nevertheless it remains one of the weak points of such systems, since couplings are effected only between preselected individual bits of different units, and in the majority of cases the binary digit values are intermediate. In addition, gain in speed is achieved exclusively through parallelism, while digital computers designed on this principle remain an inflexible system with all its inherent shortcomings.

We should note that an image processed in such a unit comprises like classes of number arrays. Therefore one of the important shortcomings of such systems is the difficulty of exchange between images corresponding to unlike classes. In this case much also depends on the element base. In the opinion of the authors, the following basic problems must be resolved in the future: 1) reduction in the power requirements of individual elements; 2) development of devices performing complex operations (calculation, etc); 3) development of devices operating in the microsecond range; 4) development of devices operating with images larger than 128 x 128.

3. Optoelectronic digital computers based on microelectronic homogeneous structures. Optoelectronics has also made it possible to approach from different positions designing of digital computers based on microelectronic homogeneous structures. These computers are constructed of identical modules consisting of identical units, each of which can perform a certain set of logic operations, whereby selection of a given operation is determined by a certain tuning signal [46]. Thus technical parameters in such devices (storage capacity, logic and computing capabilities of the blocks, links between functional units, assemblies and blocks, etc) can be program-changed (tuned) during or just prior to operation.

There exists the opinion [46] that computers based on microelectronic homogeneous structures are most efficiently utilized for organizing specific classes of control systems and production monitoring; in addition, they are least sensitive to various influences.

Every control process consists in measuring current state y with utilization of preselected system y_0 of measuring standards and obtaining difference Δy; in forming corresponding control programs $P(\Delta y)$, which change the state of the object in a direction determined by the criterion of quality. In electronics it is very difficult to organize that large number of links which are required for designing microelectronic homogeneous structures. Optical methods make it possible to sidestep this difficulty and increase the functional linkages of the circuit.

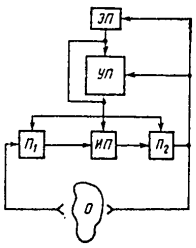

Figure 13. General Structure of a Microoptoelectronic Parallel Control System

Key:

УП -- Holographic control processor

ЭП -- Electronic console

ИП -- Executing processor

Key to Figure 13 on preceding page, cont'd:

Π_1, Π_2 -- Parallel input and output devices

O -- Controlled object

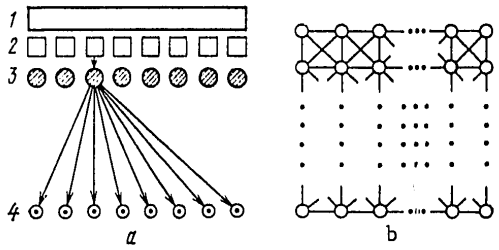

Figure 14. Diagram of Parallel Tuning and Input-Output of Operands (a) and Diagram of Linkages Between Executing Processor Cells (b)

Key:

1. Screen console with built-in (hardware) graphic input language translator
2. Matrix of laser diodes
3. Executing processor tuning and main memory hologram-microprogram carrier
4. Matrix of executing processor cells with optical input-output

The authors of [47] propose a general structure of an optoelectronic system designed to perform control tasks (Figure 13). A holographic control processor (CP) is designed on the basis of a controlled matrix of laser diodes and a matrix of hologram-microprograms (Figure 14) and is controlled by a program interpreted by control console optoelectronic circuits. Adjustment of the executive processor (EP) is effected parallel by one hologram. Control information also comes from the controlled object. Additional tuning parameters (standards, comparison logic y and y_0, etc) are fed into the matrix of the EP through the electronic console. Control programs P (Δy) are also formed with the aid of the electronic console.

The EP processor (Figure 14) is based on a homogeneous microoptoelectronic matrix [47, 48], each cell of which consists of an optical input register IN, microelectronic processing and storage circuits (including control memory) and an optical output register OUT, the outputs of which during tuning cycle are switched to the inputs of the control memory, and on input cycle -- to the cell operand memory inputs.

Such a processor makes it possible to perform operations of space and time correlation and storage of images -- basic operations essential in analyzing latent relationships and patterns. In addition, the processor matrix can also perform computing operations.

The authors of [47] present experimental results on elaboration of a homogeneous microelectronic matrix. A matrix was constructed with 4 x 4 cells, measuring 5.5 x 5.5 mm, with four optical inputs and one output in each cell. There is a total of 64 inputs, 16 outputs and some switching logic, with 33 transistors. The authors concluded that it is possible to build a matrix of 10^4 cells on a 50 x 50 mm crystal, with an operand size n x n 8-16, and speed (entire picture switching time) of one microsecond; consequently, a total of 10^6 bits of information are entered in a single cycle, that is, rate of processing is 10^{12} bits per second.

Such a system achieves complete parallelism of input-output and storage, as well as processing of topological information characteristic of the object.

Conclusion

The above-examined aspects of digital processing of information on optoelectronic devices indicate that intensive work is currently in progress on developing high-output optical computing systems.

We have examined attempts to design computing devices utilizing optical logic elements which are connected into logic circuits similar to electronic logic circuits. To achieve efficient utilization of the capabilities of parallel processing, it is suggested that in optoelectronics one employ non-positional and redundant positional systems of notation, in which carries do not go beyond one digit position.

Holographic memories are one of the first practically developed devices. On the basis of these devices one can perform various computing operations, organize associative information search, etc.

We have examined the features of optoelectronic processors. An optoelectronic processor with variable operators possesses broader functional capabilities than traditional processors. We have indicated the advantages of an optoelectronic system based on microelectronic homogeneous structures, designed for solving control problems. An optoelectronic computer based on parallel image processing of like classes of number arrays makes it possible to achieve high speed.

The purpose of these investigations is to design optoelectronic computer circuits capable of solving problems which electronic computers cannot handle, as well as improvement of the characteristics of existing computers. Modern electronic multiprocessor computer systems have an output capability in excess of 10^8 operations per second, and computers presently on the drawing board will be several times faster. Such systems are utilized with a high degree of efficiency if problem solving algorithms permit natural parallelism. There exists, however, a large number of problems which either do not possess such a property or which have no prior-known solution algorithms whatsoever. In this case employment of an electronic computer is either inefficient or impossible. The specific features of optics make it possible to design systems which can efficiently solve such problems. For

example, the above-examined optoelectronic processor with variable operators can also be employed as an adaptive computer, and its adaptivity can be manifested at the lowest level -- logical.

It follows from the above that digital optoelectronic computer devices designed for interfacing with electronic computers and for solving special problems can be practically realized in the near future. Subsequent development of the element base (controlled transparencies, optical reversing media, etc) will also make it possible to design optoelectronic computer systems as a whole, capable not only of competing with electronic computers but also of solving problems which electronics cannot handle.

BIBLIOGRAPHY

1. Mayorov, S. A., and Novikov, G. I. "Printsipy organizatsii tsifrovykh mashin" [Principles of Organization of Digital Computers], Leningrad, Mashinostroyeniye, 1974.

2. Strouk, Dzh. AVTOMETRIYA, No 5, 18, 1977.

3. Landauer, R. "Optical Information Processing (USA-USSR Seminar, 1975, Washington)," Plenum Press, New York, Vol 1, 1976.

4. Ablekov, V. K.; Zubkov, P. I.; and Frolov, A. V. "Opticheskaya i optoelektronnaya obrabotka informatsii [Optical and Optoelectronic Information Processing], Moscow, Mashinostroyeniye, 1976.

5. Basov, N. G.; Morozov, V. N.; Nikitin, V. V.; and Samoylov, V. D. RADIOTEKHNIKA I ELEKTRONIKA, 14, 1623, 1969.

6. Kartsev, A. M. "Arifmetika tsifrovykh mashin" [Digital Computer Arithmetic], Moscow, Nauka, 1969.

7. Sasaki, W.; Tanaka, T.; Kan, H.; and Shii, M. IEEE J. QE-13, 587, 1977.

8. Yacobs, Y. I. Report CLEA-1977. Washington, 1-3 June 1977 (to be published).

9. Mezz, D., and Logan, R. APPL. PHYS. LETTS, 30, 530 (1977).

10. Lee, S. H. "Optical Information Processing (USA-USSR Seminar, 1976, Washington)," Plenum Press, New York, 1977.

11. Schmidt, R. V., and Buhl, L. L. ELECTR. LETTS, 22, 575, 1976.

12. Shelton, J.; Reinhart, F. R.; Logan, R. A. APPL. OPTICS, 17, 890, 1978.

13. Sheem, S. K., and Tsai, C. S. APPL. OPTICS, 17, 893, 1978.

14. Taylor, H. F. APPL. OPTICS, 17, 1493, 1978.

15. Orlov, L. A. In the volume "Kibernetika na sluzhbe kommunizma" [Cybernetics in the Service of Communism], Moscow, Energiya, 1966, Issue 3.

16. Orlov, L. A., and Popov, Yu. M. KVANTOVAYA ELEKTRONIKA, 1, 27 (1974).

17. Orlov, L. A., and Popov, Yu. M. AVTOMETRIYA, No 6, 8 (1972).

18. Basov, N. G.; Popov, Yu. M.; Kompanets, I. N.; Morozov, V. N.; et al. FIAN Preprint, Moscow, 1973, No 3.

19. Orlov, L. A., and Popov, Yu. M. AVTOMETRIYA, No 6, 14, 1972.

20. Akushskiy, I. Ya., and Yusitskiy, D. I. "Mashinnaya arifmetika v ostatochnykh klassakh" [Computer Arithmetic in Remainder Classes], Moscow, Sov. radio, 1968.

21. Hemel, A. ELECTRONICS, 43, No 10, 104, 1970.

22. Huang, Alan. "Intern. Confer. on Opt. Computing in Research and Development," Preprints, Budapest, 1977, page 133.

23. Collins, S. A.; McKay, J. M.; and Vick, C. R. "Computer Conference, Spring, 1978," page 198.

24. Rakhmanov, V. F., and Rotar', S. L. Certificate of Invention No 257880, BI, No 36, 122, 1969.

25. Yegorova, L. V., and Rakhmanov, V. F. In the volume "Opticheskaya i elektrooptricheskaya obrabotka informatsii" [Optical and Electrooptical Information Processing], Moscow, Nauka, 1975, page 145.

26. Rakhmanov, V. F., and Rotar', S. L. Certification of Invention No 269605, BI, No 15, 122, 1970.

27. Avizienis, A. IRE TRANS., EC-10, No 3, 1961.

28. Avizienis, A. "AFEPS Conf. Proc.," San Francisco, Part I, Vol 26, 1964.

29. Sacaguhi, M.; Nishida, N.; and Nemoto, T. IEEE TRANS. C-9, 1174, 1970.

30. Knight, G. R. APPL. OPTICS, 13, 904, 1974.

31. Mayorov, S. A., and Ken, Li Si. IZV. VUZOV SER. PRIBOROSTROYENIYE, 17, 53, 1974.

32. Gibin, I. S., and Tverdokhleb, P. Ye. In the volume "Golografiya i obrabotka informatsii" [Holography and Information Processing], Leningrad, Nauka, 1976, page 5.

33. Korshever, I. I.; Matushkin, G. G.; and Tverdokhleb, P. Ye. AVTOMETRIYA, No 1, 9, 1974.

34. Akayev, A. A., and Mayorov, S. A. "Kogerentnyye opticheskiye vychislitel'nyye mashiny" [Coherent Optical Computers], Leningrad, Mashinostraoyeniye, 1977.

35. Khaykin, B. Ye. "Opticheskiye metody obrabotki informatsii" [Optical Information Processing Methods], Leningrad, Nauka, 1974, page 33.

36. Krayzmer, L. P.; Borodayev, D. A.; Gutenmakher, L. I.; Kuz'min, B. P.; and Smelyanskiy, I. L. "Assotsiativnyye zapominayushchiye ustroystva" [Associative Memories], Leningrad, Energiya, 1967.

37. Gibin, I. S.; Gofman, M. A.; Kibirev, S. F.; Pek, Ye. F.; and Tverdokhleb, P. Ye. AVTOMETRIYA, No 5, 37, 1977.

38. Tverdokhleb, P. Ye. AVTOMETRIYA, No 6, 3, 1976.

39. Morozov, V. N. KVANTOVAYA ELEKTRONIKA, 5, 7, 1978.

40. Popov, S. A.; Smolov, V. B; Ochina, L. B.; Ken, Li Si; Morozov, V. N.; and Kompanets, I. N. In the volume "Parallel'nyye mashiny i parallel'naya matematika" [Parallel Computers and Parallel Mathematics], Kiev, Znaniye, 1978, page 10.

41. Basov, N. G., et al. KVANTOVAYA ELEKTRONIKA, 5, 526, 1978.

42. Basov, N. G., et al. KVANTOVAYA ELEKTRONIKA, 5, 533, 1978.

43. Kompanets, I. N. ZARUBEZHNAYA RADIOELEKTRONIKA, No 4, 46, 1977.

44. Volodin, Ye. B., and Svidzinskiy, K. K. AVTOMETRIYA, No 4, 42, 1967.

45. Shefer, D. Kh., and Strong, Dzh. TRUDY IIER, 65, No 1, 157, 1977.

46. Prangishvili, I. V.; Abramova, N. A.; Babicheva, Ye. V.; and Ignatushchenko, V. V. "Mikroelektronika i odnorodnyye struktury dlya postroyeniya logicheskikh i vychislitel'nykh ustroystv" [Microelectronics and Homogeneous Structures for Designing Logic and Computer Devices], Moscow, Nauka, 1977.

47. Bykhovskiy, V. K.; Prangishvili, I. V.; Sonin, M. S.; and Uskach, M. A. AVTOMETRIYA, No 6, 10 1977.

48. Bykhovskiy, V. K.; Prangishvhili, I. V.; Mirzoyan, G. A.; Sonin, M. S.; and Uskach, M. A. In the book "Problemy golografii" [Problems of Holography], Issue 2, Moscow, MIREA, 1973.

Physics Institute imeni P. N. Lebedev of the USSR Academy of Sciences, Moscow
Submitted 8 June 1978

[154-3024]

PHYSICS

UDC: 621.378.325

PROPERTIES OF A LASER WITH AN UNSTABLE RESONATOR CONTAINING SMALL-SCALE PHASE INHOMOGENEITIES

Moscow KVANTOVAYA ELEKTRONIKA in Russian Vol 6 No 6, Jun 79 pp 1164-1170

[Article by L. V. Koval'chuk, V. V. Sergeyev, and V. Ye. Sherstobitov]

[Text] The authors present results of numerical calculation of fundamental mode field distribution in an unstable resonator filled with an active medium and containing small-scale inhomogeneities. The authors also present results of experiments with such resonators based on a continuous-wave CO_2 laser. The results of the investigations indicate that the presence of small-scale phase inhomogeneities on the resonator axis may lead to a sharp increase in laser radiation density within the resonator and to a substantial decrease in axial beam brightness.

The authors of [1] demonstrated that small-scale phase inhomogeneities (SPI) can under certain conditions substantially alter the properties of an unstable resonator, leading to undesirable concentration of the fundamental mode field in the vicinity of the resonator axis and to an increase in its Q. These conclusions, however, were reached for resonators not containing an active medium, since the calculations did not consider the effects of amplification factor saturation.

The purpose of this article is to investigate the properties of an unstable resonant cavity filled with an active medium under conditions where SPI are present in the cavity. In the first part of the article we shall present the results of numerical calculation of the structure of the lower mode in such a cavity. The results indicate that consideration of saturation of the medium does not lead to a substantial attenuation of the effect of fundamental mode field concentration on the axis, caused by the presence of SPI in the cavity. The second part of the article contains results of experiments with a continuous mode continuous-flow CO_2 laser, which demonstrate a substantial change in field structure in the resonator with introduction of SPI.

Our calculations, just as those in [1], were performed for the case of a two-dimensional planoconvex resonator, on the convex mirror of which is placed a

CPI simulating relief (Figure 1). With this relief, the shape of the mirror surface is described by expression

$$y = -\frac{x^2}{2R} - \delta\lambda \cos\frac{\pi n x}{a} + \\ + \Phi \equiv -\frac{x^2}{2R} - \varphi(x). \qquad (1)$$

Here and henceforth we shall use the designations adopted in [1].

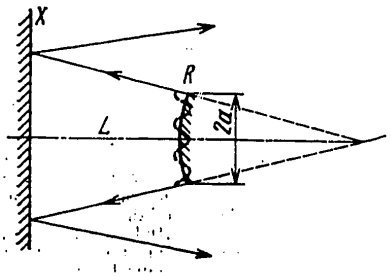

Figure 1. Diagram of an Unstable Resonator With Periodic Perturbation

We shall assume that the active medium is concentrated in an infinitely thin layer lying on the surface of the convex mirror. Such an approximation is utilized fairly extensively in calculations (see, for example, [2, 3]) and is entirely acceptable in analyzing the transverse structure of a field in unstable resonators and small values M (namely, when $M-1 \ll 1$), when the degree of nonuniformity of radiation through the volume of the resonator is small.

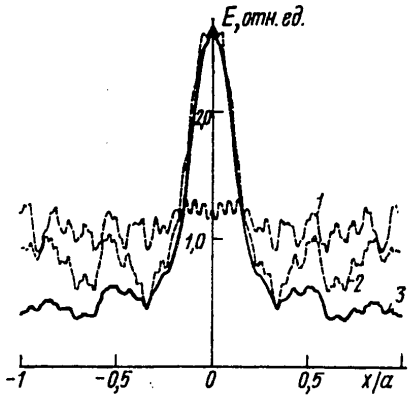

Figure 2. Distribution of Amplitude of Fundamental Mode

Let factor G (x), by which combined field amplitude E (x) is multiplied after twice passing the active medium layer, be determined by expression

$$G(x) = \exp\left[\frac{k_0 L}{1 + 2|E(x)|^2} - \sigma_0 L\right], \qquad (2)$$

where L is resonator length; k_0 and σ_0 are the weak signal amplification factor and coefficient of inactive losses in relation to a unit of resonator length.

This notation corresponds to a case, chosen for simplicity, of a fixed active medium with uniformly spread generation line; field intensity $2|E(x)|^2$ is expressed in relative units. Adopted as unit of measurement is total intensity of counterflows in the resonator, for which the amplification factor per unit of length decreases twice as much as k_0.

Taking into consideration expression (2), the amplitudes of a field of radiation incident on the concave mirror in k and (k+1) resonator passage, can be linked by relation

$$E_{k+1}(x) = \sqrt{\frac{i}{L\lambda}} \int_{-a}^{a} E_k(x') G(x') \exp\left[-\frac{i\pi M}{L\lambda}\left(x' - \frac{x}{M}\right)^2 - \right.$$
$$\left. - \frac{2\pi i}{\lambda} \varphi(x')\right] dx', \qquad (3)$$

where E (x) is the lower-mode complex amplitude registered on the equiphase surface of an outgoing wave of geometric approximation in an unperturbed resonator.

Field distribution E (x), established with an increase in the number of passages, was found by the method of iterations with the aid of a BESM-6 computer. Calculations were performed for the same set of resonator parameters and perturbing phase distortions as in [1].

As an example, Figure 2 contains lower-mode field amplitude distributions on a convex resonator mirror, calculated with the aid of (3) for a fairly typical case, where M=1.4,

$$N_{экв} = [a^2/(4L\lambda)](M - 1/M) = 7{,}5;\ k_0 L = 0{,}72;\ \sigma_0 L = 0{,}02.$$

Curve 1 gives a steady-state distribution of field amplitude on the mirror in the absence of phase disturbances. As should have been the case, the form of this distribution is fairly close to uniform, as predicted from geometric considerations.

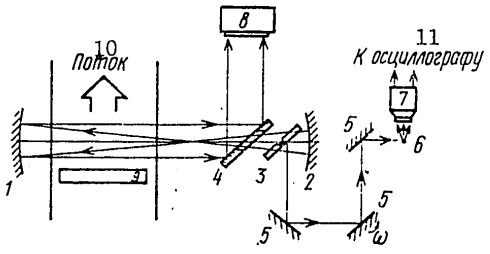

Figure 3. Diagram of Experimental Unit

Key to Figure 3 on preceding page:

1, 2. Resonator reflectors
3. Plate with SPI
4. Output mirror
5. Flat mirrors
6. Scatter
7. Cooled photodetector
8. Calorimeter
9. Discharge zone
10. Flow
11. To oscillascope

The authors of [1] demonstrated for the case of an "empty" resonator that with introduction into an unstable resonator of phase inhomogeneity of the type (1), the parameters of which satisfy the condition

$$\Phi \approx 0 \text{ и } \frac{M-1}{M+1} < \frac{\delta\pi^2 n^2}{N_{экв}} < \frac{M+1}{M-1},$$

one should observe a sharp increase in field density close to the system axis. Curve 2 in Figure 2 corresponds to a case where this condition is met (δ=0.063, n=6, Φ=0), but in contrast to the curves in [1], it is figured for a resonator filled with an active medium. A comparison of curves 1 and 2 shows that even in the presence of active medium saturation, the introduction of SPI into an unstable resonator can be accompanied by a substantial increase in radiation density on the resonator axis. In particular, in the cited example intensity of radiation on the axis increased more than fourfold.

In order to estimate the magnitude of effects induced by saturation of the medium, Figure 2 shows lower-mode field amplitude distribution on the reflector for the same phase perturbation parameters as in the case represented by curve 2, but calculated by the conventional Fox-Lee method for an "empty" resonator (curve 3). Both curves are normalized in such a manner that the amplitudes of radiation on the resonator axis coincide. As is evident from the figure, the influence of saturation reduced merely to a certain field increase on the periphery of the mirror.

We also obtained similar results for other disturbance parameters and resonator characteristics. Thus one could assume that the effect of concentration of radiation on the resonator axis should be manifested in practice in the presence of SPI in a laser with an unstable resonator. For experimental verification we undertook special investigations conducted on the basis of a continuous-flow electrical-discharge CO_2 laser with an unstable resonator. We recorded energy and spatial characteristics of laser radiation with introduction into the resonator of artificial time-stationary SPI. As was indicated in [1], the effect of field concentration on the resonator axis, induced by the presence of SPI, should be especially noticeable at high equivalent Fresnel numbers ($N_{экв} \gg 1$), that is, in those cases when, all other conditions being equal, the active medium cross section is large. In our experiments we employed a confocal unstable resonator consisting of two concave mirrors (Figure 3). All other conditions being equal, the equivalent Fresnel number of such a resonator proves to be 2M/(M-1) times that in the case of a

planoconvex resonator, the scheme of which was employed in the calculations. The resonator had the following parameters: $R_1 \approx 2.4$ м; $R_2 \approx 1.7$ м

$M = R_1/R_2 \approx 1.4$; $L = R_1/2 + R_2/2 \approx 2.05$ м.

The diameter of the aperture in the exit mirror was $2a = 18$ мм, $N_{эфф} \approx 4.5$.

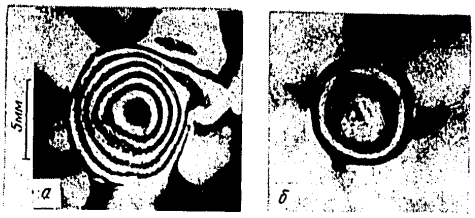

Figure 4. SPI Interferogram When $2\delta \approx 0.18$, $n \approx 2.25$ (a) and $2\delta \approx 0.06$, $n \approx 3$ (b)

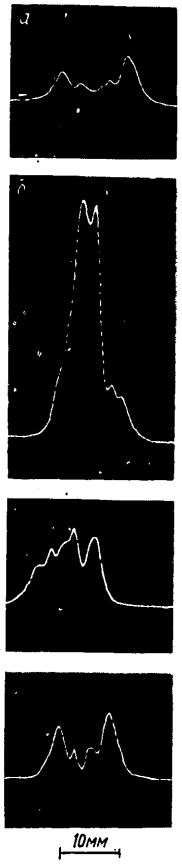

Figure 5. Distribution of Intensity by resonator Section

Key:

а. Undisturbed resonator, $2\delta = 0$

б. $2\delta \approx 0.18$

в. $2\delta \approx 0.06$

г. $2\delta \approx 0.18$

SPI is displaced 3 mm relative to the resonator axis

One can easily see that in contrast to a planoconvex resonator, where field concentration was caused by the presence of a "depression" on the mirror surface, positioned on the resonator axis in a confocal stable resonator selected by us, phase inhomogeneity of the "hillock" type on the exit concave mirror should lead to a similar effect. A like inhomogeneity was simulated in our experiments by introducing into the resonator, in the vicinity of this mirror, a plate of NaCl, on one side of which a dimple of the requisite depth and cross dimension was pressed out mechanically, with the aid of a glass lens of proper curvature. Examples of interferograms characterizing the shape of the wave front following two-time plane wave passage through the plate are shown in Figure 4 (the interferograms were obtained in light with λ=0.63 micron). If we assume that the shape of the dimples or craters approximately correspond to one period of cosine curve (1), which describes the mirror's phase relief (which of course is a very rough approximation), a plate with such inhomogeneities simulated at a laser wavelength of 10.6 microns the central part of phase relief (1) with the following parameters: $\delta \approx 0.09$, $n \approx 2.25$; $\delta \approx 0.03$, $n \approx 3$. Equivalent Fresnel numbers at the dimension of these inhomogeneities comprised ~ 0.9 and ~ 0.5 respectively. Thus the condition of formation on the axis of a stable resonator system (see [1]) was met, and introduction of these inhomogeneities should have been accompanied by an increase in density of radiation on the resonator axis and a decrease in generation threshold.

The experiment was set up in such a manner that the plate on which phase inhomogeneities were introduced could displace translationally in a direction perpendicular to the resonator axis. Both an unperturbed resonator and a resonator containing any of the phase inhomogeneities could be obtained without changing mirror alignment, positioning the plate either precisely on the resonator axis or at any preselected distance from it.

Distribution of radiation intensity on an axial section of the resonator parallel to the direction of flow was recorded on an oscillascope with the aid of a scanning system previously utilized in [4]. A second surface of the plate simulating SPI, free of disturbances, was employed to tap a portion of the radiation into this system.

Figure 5a contains an oscillogram demonstrating the structure of the field in the vicinity of the exit mirror of a resonator in which inhomogeneities are not present. The field structure is close to symmetrical, which is characteristic of resonators effecting "mixing" of radiation propagating along both sides of the axis [4]. The intensity "trough" by the resonator axis is due to nonuniformity of the amplification factor, which drops off rapidly during gas movement through a resonator (e times at a length of $\sim$12 mm).

Figure 5б, в contain field distribution oscillograms obtained while introducing onto the resonator axis SPI the interferograms of which were shown in Figure 4a, б. It follows from these oscillograms that even in the case of Figure 5в, corresponding to a "hillock" height on the mirror surface of only 0.06 λ, one observes a substantial change in field structure in the resonator and an increase in average power of radiation incident on the exit mirror. In the

case represented in the oscillogram of Figure 5б (equivalent "hillock" height on the mirror is ~0.18 λ), the presence of effect of field concentration on the resonator axis during the introduction of SPI is without question. It is interesting to note that in all three cases (Figure 5, а-в) the laser radiated power differed insignificantly (this question will be discussed below in greater detail).

As was shown in [1], the effect of field concentration in a resonator should arise only when an SPI is located on or in the immediate vicinity of the resonator axis. Indeed, only in these cases can such small phase distortions lead to the formation of a local stable resonator. This is confirmed by an oscillogram (Figure 5г) which was obtained with the same inhomogeneity as in the case of Figure 5б, but the inhomogeneity proper, the lateral dimension of which was ~8 mm, was displaced 3 mm in a transverse direction. As is evident from the oscillogram, the effect of field concentration on the axis indeed disappears, while distribution of intensity along the section approximates distribution in an undisturbed resonator.

The calculations in [1] attested to the fact that with a field concentration on the axis caused by the presence of SPI in the resonator, the wave front of the basic mode became substantially deformed. Evidently in experiments this should be manifested in decreased axial brightness of radiation. Quantitative investigations of beam angular divergence were not performed in this study. However, a qualitative judgment of a substantial decrease in axial radiation brightness with the introduction of SPI on the resonator axis can be made from a comparison of beam profiles in the mirror focal plane, obtained by focusing radiation onto a transparent plastic plate (Figure 6). Figure 6а corresponds to a case of an undisturbed resonator, while Figure 6б represents the form of a focal spot with the presence of SPI in the resonator, causing field concentration on the axis (Figure 5б). Both focal spots were obtained with practically the same power level and different exposure times.

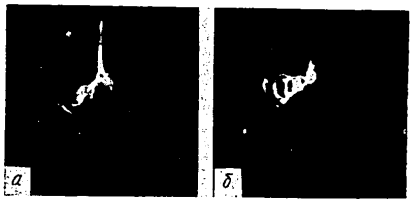

Figure 6. Photograph of a Laser Radiation Focal Spot

Evidently with the presence of many SPI in a resonator the field concentrates on the axis whenever there is an SPI on the resonator axis capable of making the resonator stable in the axle-adjacent region. We should also note that when an opposite-sign inhomogeneity appears on the resonator axis, as well as in all intermediate cases, substantial local decrease in field density on the

resonator axis does not occur [1]. Thus one can state that with the presence in a resonator of SPI which change on a time axis in a random manner, the average radiation density, in time, in the central zone adjacent to the axis may prove to be greater than in an undisturbed resonator.

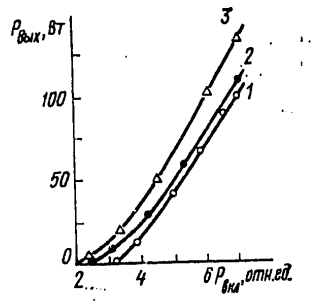

Figure 7. Dependence of Output Power on Pumping Power

This circumstance must be taken into consideration when designing resonators and analyzing the results of experiments performed with rapid-flow lasers, characteristic of which is a comparatively high level of active medium density pulsations.

Presenting similar arguments applicable to radiation angular divergence, one can state that time-average axial brightness with the presence of random SPI in the resonator, characterized by a certain set of scales and phase advances, will depend on the magnitude of axial brightness achieved with precise localization on the resonator axis of the individual types of SPI present in the medium and on the relative probability of their occurrence in the axial-adjacent zone.

Thus time-average axial brightness with the presence of SPI should always be less than the brightness achieved in their absence.

As was shown in [1] for an "empty" resonator, field concentration of the axis, caused by the presence of SPI in the resonator, is accompanied by a significant drop in the level of basic mode losses, which in an actual laser should be expressed in a drop in the generation threshold. Figure 7 contains experimental curves of relationship between laser power output and pumping power for an undisturbed resonator (curve 1) and with introduction of the inhomogeneities represented by the interferograms in Figure 4a, б (curves 3 and 2 respectively). It follows from this figure that the presence on the resonator axis of SPI, which introduce a difference in travel per passage of only several hundreds of a wavelength indeed leads to an appreciable lowering of the generation threshold. The nonlinear character of energy relations in the region of the threshold attests to change in the field structure with increased pumping and a related increase in losses of oscillations of the

fundamental type. It is evident from the graph that with low pumping levels a lowering of the generation threshold is accompanied by a substantial change in laser output power. It is clear that with movement of such inhomogeneities relative to the resonator axis, in this case one should observe laser output power pulsations. It is quite probable that precisely such a mechanism of pulsations is sometimes realized in flow-through gas lasers with a high level of active medium turbulence and low amplification factors. With greater surpassing of the generation threshold, changes in output power caused by SPI should become increasingly less appreciable. This is due to the fact that, as we know, output power changes little during variation of active losses across a fairly broad range if their initial value was close to optimal. In our experiments the small power gain observed with the introduction of SPI was connected with the fact that in the initial state the resonator axis, in order to reduce optical inhomogeneities, was displaced downflow from the zone of mixing of air with carbon dioxide, and therefore the increase M=1.4 slightly exceeded the optical value for this case.

In conclusion we can state that the results of this study attest to the fact that SPI, as was assumed in [1], can significantly influence the properties of lasers with unstable resonators. This circumstance must be taken into consideration both in developing actual lasers and in analyzing experimental results.

The authors express their thanks to Yu. A. Anan'yev for a number of valuable comments which prompted these investigations.

BIBLIOGRAPHY

1. Koval'chuk, L. V., and Sherstobitov, V. Ye. KVANTOVAYA ELEKTRONIKA, 4, 2166 (1977).

2. Statz, A., and Tank, C. L. J. APPL. PHYS., 36, 1816 (1965).

3. Rensch, D., and Chester, A. APPL. OPTICS, 12, 997 (1973).

4. Anan'yev, Yu. A.; Kuprenyuk, V. I.; and Sherstobitov, V. Ye. KVANTOVAYA ELEKTRONIKA, 4, 1456 (1977).

Submitted 5 May 1978;
reworked and resubmitted 8 August 1978

[154-3024]

PHYSICS

UDC: 621.378.33

EXPERIMENTAL AND THEORETICAL STUDIES OF A CLOSED-CIRCUIT GAS-DYNAMIC CO_2 LASER

Moscow KVANTOVAYA ELEKTRONIKA in Russian Vol 6 No 6, Jun 79 pp 1171-1175

[Article by G. M. Klepach, V. F. Konakh, V. A. Soldatov, and V. F. Sharkov]

[Text] The authors report development of a continuous-wave gas-dynamic CO_2 laser with closed-circuit circulation of the CO_2-N_2-He gas mixture. Operating parameters of the system are as follows: gas temperature $\lesssim$1200°K; compression ratio $\sim$6; gas consumption $\lesssim$ 1 kg/s. Measured gain value is $\sim$0.25 m^{-1}. The authors show that with utilization of a closed circuit overall efficiency of the laser system can be substantially increased, which is extremely important for practical employment of such devices in materials processing and in metallurgy.

At the present time gas-dynamic CO_2 lasers continue to be intensively investigated, both theoretically and experimentally [1-6]. Principal attention is focused on development of systems with pulse ($\tau \approx 1$ ms) and quasi-continuous ($\tau \approx 1$-5 s) operating modes, which is evidently connected with the technical simplicity of such devices. It seems obvious, however, that for practical employment the most promising are lasers with closed-circuit circulation of working medium, in which no gas is ejected into the atmosphere and where it is possible to obtain a high laser efficiency [7-11], which in the final analysis leads to savings in power requirements.

Using such a laser system, built at the Institute of Atomic Energy imeni I. V. Kurchatov, we study the influence of the design features of individual laser components (nozzle unit, diffusor, etc) on the operating characteristics of a GDL during protracted ($\tau > 10$ min) working medium circulation through a closed circuit.

Measurement results were compared with theoretical calculations and experimental data obtained on an open-cycle laser with similar temperature, pressure and mixture composition parameters [6].

Description of Experimental Unit

The unit (Figure 1) comprises a closed, sealed circuit through which the working medium circulates: a mixture of CO_2-N_2-He gases. The mixture, compressed in six-stage centrifugal compressor 8, passes through pipes into regenerator 3, where it is heated with a counterflow of hot exhaust gas to T≈750°K. Then the gas, passing through to sequentially-linked heater sections 1, which provide the capability to heat to a temperature of approximately 1200°K, enters working channel 2, where it is accelerated in a nozzle unit to a velocity of M=3-3.5. The "freezing" of the N_2 and CO_2 (001) oscillation levels which occurs creates conditions for generating in the resonant cavity radiation with a wavelength of 10.6 microns.

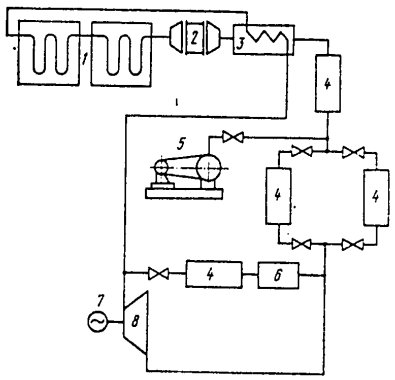

Figure 1. Schematic Diagram of Unit

The supersonic flow is retarded in the diffusor, after which, passing through regenerator 3 and cooler 4, it cooled to 20°C and enters the compressor. Preparation of the working mixture for filling the circuit and continuous leak compensation is handled in a special tank. The circuit contains a bypass line with cooler 4 and filter 6 for continuous mixture purification. Evacuation system 5 ensures that the circuit remains clean and guarantees uniformity of mixture composition. Compressor unit 8, with a compression ratio of approximately 6 on mixtures with helium, has two intercoolers and is powered by induction motor 7.

The heater, designed for maximum power requirements of 180 kilowatts, consists of two sections, the heating elements of which comprise a polished pipe of high-temperature KhN70Yu alloy. The tube is heated by passing alternating current directly through it.

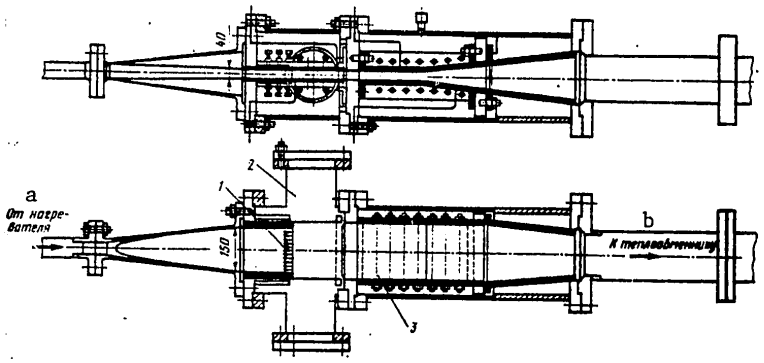

Figure 2. Sketch of GDL Gas Flow Channel

Key:
a. From heater
b. To heat exchanger

The working section (Figure 2) consists of a prechamber, nozzle unit 1, resonator 2, and diffusor 3. The nozzle unit consists of 25 flat shaped nozzle vanes with critical section height of 0.8 mm. Preliminary nozzle grid blow-throughs on an aerodynamic test stand confirmed the previously-calculated character of flow beyond the nozzle ($M \approx 3.5$). The optical resonant cavity has dimensions of 3 x 15 x 10 cm. In addition to monitoring circuit operating characteristics: static pressure, temperature, flow rate, we measured gain K_0 at a distance of 2 cm from the nozzle exit according to change in intensity of a reference radiator.

Discussion of Results

Following are the results of measurement of parameters of the GDL closed circuit and gain.

Composition of working mixture, mole	$2CO_2$-$5N_2$-3He
Heater wall temperature, °K	1270
Gas stagnation temperature at working section inlet, °K	950
Pressure in prechamber, atm	4.2
Pressure in resonator, atm	0.1
Pressure at compressor inlet, atm	1.02
Pressure at compressor outlet, atm	5
Temperature at compressor inlet, °C	20
Temperature at compressor outlet, °C	80
Gas flow rate, kg/s	0.35
Gain, m^{-1}	0.25

As follows from the above figures, the ratio of static pressures in the resonator and prechamber is 0.024, which corresponds to a Mach number at the resonator inlet of M=3.1. At these flow velocities and a retardation temperature of ~1000°K one can obtain specific radiation energy F=4-6 kJ/kg (K_0=0.3-0.6 m^{-1}) [3, 4, 6].

Employment of relatively low stagnation temperatures impedes obtaining large power outputs in a GDL but makes it possible to avoid designing and engineering difficulties, such as pipe cooling, employment of costly structural materials for the circuit, CO_2 dissociation, etc. In addition, one obtains a fairly long service life for individual assemblies, greater reliability and simpler maintenance. Judging from the measured gain of K_0=0.25 m^{-1}, the energy stored in the resonator is comparable with the prior-calculated energy, and in addition one should note the good stability of gain during the entire time of equipment operation. The discrepancy between the experimental and theoretical values of K_0 is evidently due to the nonoptimal section in which gain was measured, as well as the presence of stagnant zones of hot absorbing gas in resonator "pockets."

We shall estimate the theoretical gain in efficiency from the employment of such a closed circuit [10, 11]. Electrical energy fed to the working medium per unit of mass can be determined with the following formula:

$$E=c_p[m(T_5-T_4)+T_1-T_q], \qquad (1)$$

where m is the number of compressor stages separated by intercoolers; T_4, T_5 -- temperatures at compressor inlet and outlet*; T_1 -- temperature at nozzle unit inlet; T_q -- temperature at heater inlet; c_p -- heat capacity of the mixture at constant pressure. This same energy, with an open circuit, is equal to

$$E=c_p\ (T_1-T_0), \qquad (2)$$

where T_0 is the ambient temperature.

With identical specific laser power output, the ratio of efficiencies of closed and open circuits is inversely proportional to the ratio of power inputs:

$$\overline{\eta}=(T_1-T_0)/[m(T_5-T_4)+T_1-T_q]. \qquad (3)$$

With adiabatic compression in the compressor

$$T_5=T_4[(x_i-1)/\eta_K+1];\ x_i=\pi_{k_i}^{(k-1)/k}, \qquad (4)$$

where π_{ki} is the degree of compression in a compressor stage; η_k -- compressor adiabatic efficiency.

* It is assumed that the temperatures are identical at the inlets and outlets of all compressor stages.

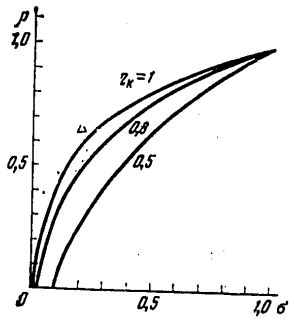

Figure 3. ρ-σ Diagram for m=3

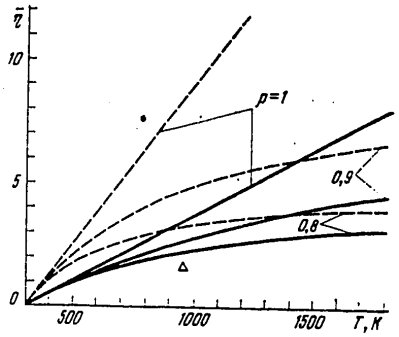

Figure 4. Dependence of $\bar{\eta}$ on Temperature at Gas-Dynamic Laser Input When T_4=3000 °K, m=3, η_k=0.8, and σ =0.2 (solid lines) and 0.5 (dashed lines) (Δ -- experimental value)

Obviously $\pi_{k_i}^m = 1/\sigma$, where σ is the circuit total pressure recovery coefficient.

Temperature T_q is linked to degree of regeneration ρ by a simple relation:

$$T_q = T_5 + \rho(T_1 - T_5). \qquad (5)$$

Substituting expressions (4) and (5) in formula (3), we finally obtain

$$\bar{\eta} = \frac{1 - T_0/T_1}{(1-\rho) + (T_4/T_1)\{[(x_i - 1)/\eta_k](m - 1 + \rho) + \rho - 1\}} \equiv \frac{1 - T_0/T_1}{(1-\rho) + B}. \qquad (6)$$

In that case where $B>0$, to increase $\bar{\eta}$ temperature at compressor input (cycle lowest temperature) should be decreased to the level $T_4=T_0$. When $B<0$ it is advantageous to increase temperature T_4 to the maximum possible, determined from condition $T_5=T_1$. Such an arrangement was proposed in [7, 8]. It does not contain a regenerator, and the formula for $\bar{\eta}$ has the form

$$\bar{\eta}=(1-T_0/T_1)[1+\eta_к/(x_i-1)]m^{-1}. \qquad (7)$$

Figure 3 contains solutions for equation B=0 for various compressor efficiencies. In the upper region $B>0$, and in the lower -- $B<0$. A triangle marks the point corresponding to experimental values of parameters ρ and σ. Figure 4 shows dependence $\bar{\eta}$ on temperature at nozzle unit inlet. One can see a sharp influence on increase in $\bar{\eta}$ by pressure losses through the circuit and degree of regeneration.

It follows from formula (6) that when $B\geq 0$

$$\lim_{T_1\to\infty}\bar{\eta}=\frac{1}{1-\rho}. \qquad (8)$$

Thus in order to increase the efficiency of the closed circuit it is necessary first and foremost to increase the degree of regeneration and reduce pressure losses.

In our experiments the diffusor total pressure recovery coefficient was 0.26, that is, approximately corresponded to the pressure recovery coefficient in a straight jump (σ=0.3). Evidently this value is not maximum and can be increased, for example, by utilizing a controlled diffusor [12]. We should also like to draw attention to the necessity of cooling the flow channel, nozzle blades and resonator cavity. The channel heated to 800°K during operation; the nozzle blade cascade, although GDL temperature conditions were taken into account in its design, nevertheless showed deformation from thermal expansion.

In conclusion we must emphasize that a GDL with working medium circulation through a closed circuit can have a high efficiency only if at the same time the entire aggregate of the system's operating parameters have been selected in an optimal manner. Therefore one can clearly see the inadvisability of developing GDL closed circuits for studying physical processes in the active medium of CO_2 lasers, which always involve the necessity of varying operating parameters across the broadest range.

On the basis of conducted investigations one can conclude the technical possibility of designing a continuous-wave industrial CO_2 gas-dynamic laser operating under prior-selected optimal operating conditions. In our opinion the high efficiency of such a GDL will compensate for the cost of engineering a closed circuit.

BIBLIOGRAPHY

1. Anderson, J. D., and Harris, E. L. AIAA PAPERS, No 72-143, 14 (1972).

2. Anderson, J. D. AIAA J., 12, 1699 (1974).

3. Krasitskaya, L. S.; Napartovich, A. P.; and Sharkov, V. F. TVT, 11, 1155 (1973).

4. Napartovich, A. P., and Sharkov, V. F. TVT, 12, 659 (1974).

5. Losev, S. A., and Makarov, V. N. KVANTOVAYA ELEKTRONIKA, 1, 1633 (1974); 2, 1454 (1975); 3, 960 (1976).

6. Abrosimov, G. V.; Vedenov, A. A.; Vitshas, A. F.; Napartovich, A. P.; and Sharkov, V. F. TVT, 13, 865 (1975).

7. Tulip, J., and Seguin, H. J. APPL. PHYS., 42, 3393 (1971).

8. Hertzberg, A.; Christiansen, W. H.; Johnson, E. W.; and Ahlstrom, H. G. AIAA PAPER, No 71-106, 16 (1971).

9. Karnyushin, V. N., and Soloukhin, R. I. FIZIKA GORENIYA I VZRYVA, 8, 163 (1972).

10. Soldatov, V. A. Preprint IAE-2966, 1978.

11. Soldatov, V. A. Preprint IAE-2975, 1978.

12. Merkly, P. E. AIAA J., 14, 168 (1976).

Institute of Atomic Energy imeni
I. V. Kurchatov, Moscow
[154-3024]

Submitted 9 June 1978

PHYSICS

UDC: 621.378.33

STUDY OF COOLED ELECTROIONIZATION CO LASER. I. LASER ACTION WITH PURE CARBON MONOXIDE

Moscow KVANTOVAYA ELEKTRONIKA in Russian Vol 6 No 6, Jun 79 pp 1208-1214

[Article by N. G. Basov, V. A. Danilychev, A. A. Ionin, V. S. Kazakevich, I. B. Kovsh, and N. L. Poletayev]

[Text] For the first time an experimental study has been made of threshold, energy, temporal and spectral characteristics of a pulsed cooled electroionization laser utilizing pure carbon monoxide (CO-EIL). Experiments were performed on a system with an active volume of approximately 5 liters, with a working gas temperature of ~100°K and density to 1.0 Amagat unit. Duration of excitation varied from 30 to 300 microseconds. Laser action was observed in a spectral region of 5.1-5.5 microns, and with an increase in pump energy the spectrum broadened into the short-wavelength region. The authors demonstrated that the efficiency of a CO-EIL employing pure carbon monoxide does not exceed 10%. It is noted that the measured parameters of the CO-EIL do not correspond to the results of theoretical calculations.

A CO laser is a complex multilevel system, for a quantitative description of which it is necessary to obtain a system solution from several dozen kinetic equations [1]. The complexity of theoretical calculations of the characteristics of a CO laser employing mixtures of carbon monoxide with helium, argon, nitrogen and other buffer gases increases appreciably in comparison with a pure CO laser due to an increase in the number of kinetic equations, indeterminacy of the constants of the processes of excitation and deexcitation in the laser mixtures, and an increase in the number of parameters characterizing broadening of the quantum transitions and the chemical processes taking place in the electrical discharge plasma. Therefore in theoretical studies calculations are performed primarily for pure CO. Of considerable interest in connection with this, from the standpoint of comparing experimental and theoretical results, is investigation of generation in an electroionization laser (CO-EIL) without the addition of buffer gases into the carbon monoxide.

Pulse generation with pure carbon monoxide was observed previously in low-pressure gas-discharge lasers [2] and in TEA lasers at room [3] and cryogenic [4, 5] temperatures. As a consequence of the low efficiency of excitation of vibrational energy levels with independent discharge in pure CO, the emission energy of these lasers (0.1-0.5 mJ) and efficiency (fractions of a percent) were low. Detailed calculations of the generation characteristics of TEA lasers employing carbon monoxide and a comparative analysis of experimental and theoretical data had not previously been performed. Employment of the electroionization method for pumping CO lasers made it possible substantially to improve the energy characteristics of such lasers [6-8], which in turn prompted theoretical investigations of this system. Laser action in a CO EIL employing pure carbon monoxide was noted in [7], but up to this time no consistent experimental study of the parameters of an EIL employing pure CO had been performed.

Our experiments were performed on a unit with cooled liquid nitrogen with an active volume of ~5 l. A description of this unit is contained in [9], and its principal operating characteristics are the following: current density in the electron beam on entering discharge gap -- to 15 mA/cm^2; energy of fast electrons beyond separating foil -- ~100 keV; excitation pulse duration, determined by active medium ionization time, varies smoothly from 5 to ~300 microseconds; density of the working gas mixture runs to 3 Amagat units; temperature in the active region when filled with pure CO is 100°K; reduced field strength in discharge gap E/N to 5 kV/(cm·Amagat units). The inner hemispherical laser resonator was formed with a concave copper mirror and interference dielectric mirror on a CaF_2 backing. Experiments were performed under the same laser pumping conditions for which calculations of generation characteristics of an EIL with pure CO were performed earlier [1].

Figure 1 contains typical oscillograms of discharge current and voltage. Change in field intensity in the discharge gap during discharge did not exceed 20-30%. Maximum excitation time values with a fixed electron beam current as well as parameter E/N and specific power input were limited by discharge gap breakdown. When pumping energy exceeds a certain threshold value, determined only by the capacitance of the bank of capacitors supplying the discharge, and gas density, it leads to gap breakdown, occurring initially with a delay of hundreds of microseconds in relation to termination of the volume excitation pulse. With a further increase in $Q_{вкл}/N$ by a quantity in the order of 10-20 J/(l·Amagat), discharge instability development time decreases sharply, and breakdown occurs prior to termination of the electron beam current pulse (see Figure 1). Maximum quantity of reduced power input under conditions of the experiment comprised ~400 J/(l·Amagat).

The generation threshold for $\alpha_{\text{п}} \sim 1.5 \cdot 10^{-3}$ cm^{-1} was reached with a specific power input of ~140 J/(l·Amagat), and in the investigated range of gas densities (0.1-1 Amagat) proved to be practically independent of density (Figure 2). Such a character of dependence $Q_{\text{п}}/N$ on N qualitatively agrees well with the results of theoretical study [10]. Measured value $Q_{\text{п}}/N$ satisfies the estimates of this study. Measurement of generation threshold for exit mirrors with differing reflection coefficients made it possible to

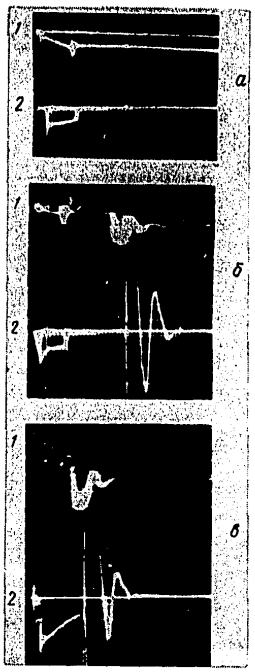

Figure 1. Typical Oscillograms of Voltage Pulses at Discharge Gap (1) and Discharge Current (2) in the Absence of (а) and With the Occurence of (б, в) Discharge Gap Breakdown

$Q_{вкл}/N \approx 370$ (а), 400 (б) and J/(1 x x Amagat)(в); sweep 50 micros/div; N=0.5 Amagat

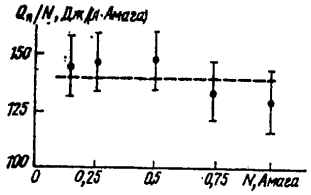

Figure 2. Relationship Between Reduced Threshold Pumping Energy and Carbon Monoxide Density When $\tau_{изл}$=30 microseconds, $\alpha_п \sim 1.5 \cdot 10^{-3}$ cm^{-1}, R=80%.

deterine the dependence of gain α_y in a CO-EIL on pumping energy (with an accuracy to the magnitude of nonresonant losses γ) (Figure 3). Gain, beginning with a certain value $Q_{вкл}/N$, increases practically linearly with an increase in energy input, reaching a value of $\sim 4 \cdot 10^{-3}$ cm^{-1} when $Q_{вкл}/N$ 200 J/(1·Amagat).

Laser action

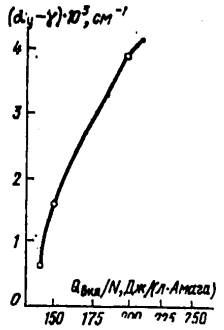

Figure 3. Dependence of Gain on Specific Energy Input When $\tau_{изм}$ =30 microseconds; N=0.5 Amagat

Laser action was observed in the region 5.1-5.5 microns (Figure 4) at vibrational transitions from 11→10 to 7→6. In our experiments we employed measuring equipment with a resolution of ~5 cm^{-1}, which permitted recording only vibrational bands taking part in laser action. Identification of the band was performed in an assumption based on the results of [1], that under experimental conditions rotational quantum number j ~10-15.

When the threshold is slightly exceeded, generation develops in three vibrational bands, and with an increase in pumping energy the number of generating vibrational bands increases, and the spectrum broadens in the direction of shorter wavelengths. The generation spectrum shift into the short-wavelength region can be explained if one assumes, in conformity with the results of theoretical study [1], that distribution of CO molecules by vibrational levels coincides with Treanor's [11] from zero to the lowest of the system of levels taking part in laser action, and the number of this lowest vibrational level corresponds to the minimum of Treanor's distribution:

$$v_H \approx \ln\left(\frac{N_0}{N_1}\right)\frac{kT}{2\omega_e x_e},$$

where N_0 and N_1 are the population densities of the zero and first levels of the CO molecule; T -- kinetic gas temperature; $\omega_e x_e \approx 27$ cm^{-1} -- anharmonicity constant. It is evident from the formula that with an increase in the population density of first vibrational level N_1, growth of which is directly linked with a pumping increase, vibrational level number v_H decreases, that is, the boundary of the generation spectrum shifts into the shorter-wavelength region.

Numerical calculation of the generation characteristics of an EIL employing pure CO performed by A. F. Suchkov and B. M. Urin predict that with an increase in pumping energy the radiation energy distribution maximum shifts along the spectrum into the shorter-wavelength region, but such a shift was not observed in our experiments.

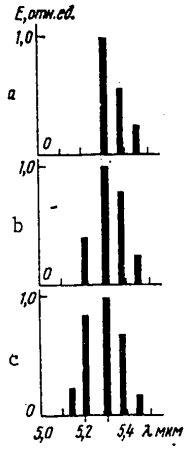

Figure 4. Distribution of Emission Energy CO-EIL Spectrum With $Q_{выд}$ /N=280 (a), 340 (b), 400 J/(1 ·Amagat) (c); N=0.5 Amagat, $\tau_{возб}$ = 100 microseconds.

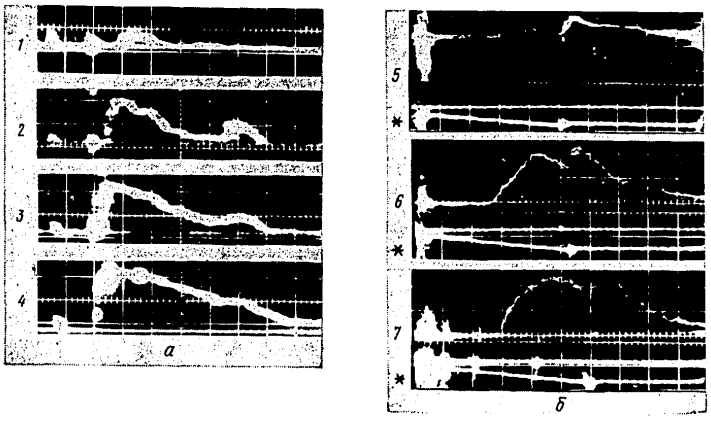

Figure 5. Oscillograms of Radiation Pulses of a CO-EIL Employing Pure Carbon Monoxide, With $\tau_{возб}$ =30 (a) and 150 microseconds (б):

N=0.5 Amagat, $\alpha_п$ $4 \cdot 10^{-3}$ cm^{-1}, sweep -- 25 microseconds/div; $Q_{выд}$ /N=200 (1, 5), 220 (2), 250 (3, 6), 300 (7) and 320 J/(1 ·Amagat) (4); * -- discharge voltage

Change in pumping energy exerts considerable influence not only on the spectral but also temporal characteristics of radiation: generation pulse duration and delay $\tau_з$ relative to excitation initiation. Generation dynamics were investigated with

$$\tau_{возб} \gtrless \tau_0.$$

Laser action in pure CO takes place with considerable delay relative to pumping pulse initiation. When pumping energy slightly exceeds threshold, the generation pulse has a peak structure (Figure 5) caused by sequential initiation of generation in different vibrational bands of the CO molecule. With an increase in pumping energy, the generation pulse becomes transformed and the peak structure disappears. Delay time $\tau_з$ of onset of generation relative to initiation of pumping with a gas density of N=0.5 Amagat and excitation time 30 microseconds, decreases from 60 approximately 25 microseconds with an increase of $Q_{вкл}/Q_{п}$ from 1 to 1.75 (Figure 6). Radiation pulse duration $\tau_и$ (at half-height) more than doubles thereby: from 40 to 100 microseconds, and exceeds by approximately fivefold the calculated generation pulse duration [12]. Further growth in pumping energy right up to $Q_{вкл}/Q_{п} \sim 2.5\text{-}3$ does not lead to an increase in generation pulse duration.

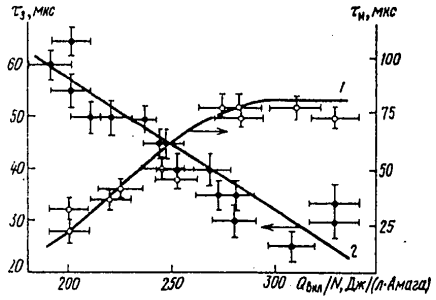

Figure 6. Dependence of Radiation Pulse Duration $\tau_и$ (1) and Generation Pulse Delay time $\tau_з$ (2) on Specific Pumping Energy With $\tau_{возб}$ =30 microseconds; N=0.5 Amagat; $\alpha_п = 4 \cdot 10^{-3}$ cm^{-1}

An increase in carbon monoxide density with constant values of parameter $Q_{вкл}/Q_{п}$ and threshold gain leads to a decrease in generation duration (Figure 7), which is evidently connected with an increase in the rate of VV-exchange, which leads to an increase in rates of formation of inversion and radiation decay of the upper laser level.

With an increase in excitation time to 100 microseconds and more, duration of laser action increases to 150-200 microseconds. While when $\tau_{возб} < \tau_з$ the radiation pulse shape is independent of the pumping pulse paramaters, when $\tau_{возб} > \tau_з$ one observes a jump in intensity of laser action at the moment discharge ends (see Figure 5б). A like effect is also

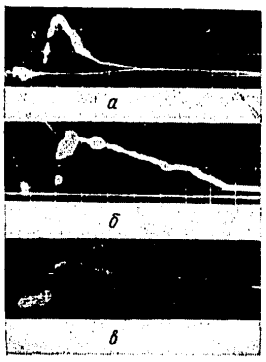

Figure 7. Oscillograms of Radiation Pulses of CO-EIL With Carbon Monoxide Densities N=1 (a), 0.5 (б) and 0.15 Amagat (в); $Q_{вкл}/Q_{т}$ =1.5; $\tau_{изл}$ = 30 microseconds; sweep 25 microseconds/div.

observed in low-pressure pulse gas-discharge lasers [2], and not only in the spectrum-integral radiation pulse but also at individual vibrational-rotational transitions. Most probably this effect, as stated in [2], is caused by deexcitation of CO vibrational levels by electron impact. With this mechanism discharge cessation and decrease of electron concentration should lead to improvement in conditions of laser action and an increase in radiation power, which was in fact observed in the experiments.

In the range of energy inputs studied, the dependence of radiated energy on parameter $Q_{вкл}/N$ is close to linear. Maximum complete emitted energy in the experiment was reached at a density of N=0.5 Amagat and comprised ~40J, which corresponds to specific power output $Q_{изл}/N \approx 13$ J/(1 ·Amagat) (obtained with $\alpha_{п}=4\cdot10^{-3}$ cm^{-1}). Further energy growth was limited as a consequence of attainment of maximum energy input into the volume discharge for the conditions of the experiment and development of breakdown.

Maximum efficiency at N=0.5 Amagat was ~3% ($\alpha_{п}=4\cdot10^{-3}$ cm^{-1}). Dependences of specific radiated energy $Q_{изл}/N$ on specific pumping energy $Q_{вкл}/N$, close to linear, were recorded at various gas densities N from 0.15 to 1 Amagat (Figure 8). Maximum radiated energy at all gas densities comprised several tens of joules. Maximum efficiency of ~10% was obtained at a density N=0.15 Amagat and specific power output ~40 J/(1 ·Amagat).

The experiments conducted to study a CO-EIL employing pure carbon monoxide showed that practically all CO-EIL parameters recorded in the experiment: gain, specific power output, efficiency, radiated pulse duration, pulse spectral composition, fail to match the results of theoretical calculations

[1, 12], performed for a laser employing pure carbon monoxide. Since the impurities contained in the industrial-grade carbon monoxide used in the experiments (N_2 -- 0.3%; O_2 -- 0.36%; Ar -- 0.04%) do not extinguish the laser effect, while possible contaminants (oil fumes, iron pentacarbonyl, etc) freeze out in a trap at nitrogen temperatures, the experiment results give reason to assume that the theoretical calculations of the kinetics of laser action in pure carbon monoxide require refinement.

The most probable reason for the discrepancy between theory and experiment is overstatement in calculations of the efficiency of vibrational excitement of CO molecules in an electrical field [13], which is computed on the basis of constants of elementary processes, which in turn are calculated theoretically. For pure CO the calculated value of pumping efficiency in the region of optimal field strengths is ~90%. One can easily see that a small difference (~10-15%) between actual and calculated efficiency signifies that the fraction of energy expended on excitement of translational degrees of freedom in CO, that is, on direct heating of gas increases by practically double. With a specific power input of ~400 J/(1 · Amagat) this additional portion of energy comprises ~40-60 J/(1 · Amagat), which corresponds to an additional temperature rise of 40-60°K during pumping.

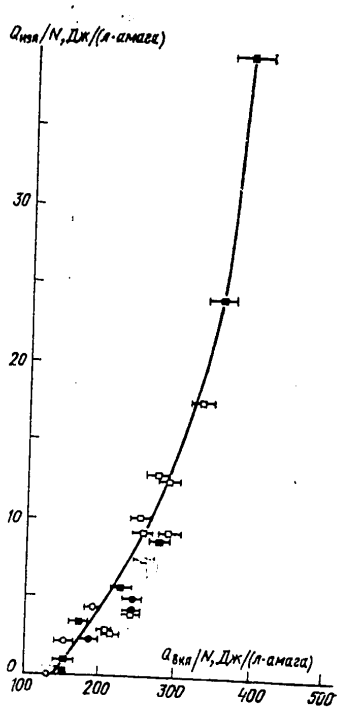

Figure 8. Dependence of Specific Radiated Energy on Specific Pumping Energy for Various Densities of Carbon Monoxide

N=1 Amagat, C=18 mfd (0); 0.5 and 18 (●); 0.25 and 18 (□); 0.15 and 51.3 (■) respectively; $\alpha_n \sim 1.5 \cdot 10^{-3}$ cm^{-1}; $\tau_{изл}$ = =30 microseconds.

An increase in the temperature of the active medium of a CO-EIL from 100 to 150 °K leads to an increase in threshold pumping energy by approximately double [14] and correspondingly to a sharp decline in pumping exceeding threshold. As a result gain, radiated energy and laser efficiency drop off appreciably (in comparison with the calculated figures for 90% effectiveness).

Absence of a shift of the energy distribution maximum through the generation spectrum into the shorter-wavelength region may also be due to a temperature increase, since a temperature increase leads to an increase in the number of the lowest vibrational level taking part in laser action, and to spectrum redistribution of radiated energy.

The hypothesis of a decrease in CO-EIL output parameters due to the presence of the isotopes $^{13}C^{16}O$ and $^{12}C^{18}O$ in the natural gas with less distances between adjacent vibrational levels [12] requires experimental verification.

In conclusion, the authors express thanks to A. P. Lobanov, A. F. Suchkov, and B. M. Urin for their discussion of the results of this study.

BIBLIOGRAPHY

1. Basov, N. G.; Dolinina, V. I.; Suchkov, A. F.; and Urin, B. M. FIAN Preprint, Moscow, 1976, No 1; KVANTOVAYA ELEKTRONIKA, 4, 776 (1977).

2. Anokhin, A. V.; Markova, S. V.; and Petrash, G. G. KVANTOVAYA ELEKTRONIKA, 1, 2239 (1974).

3. Osgood, E. W., Goldhar, J.; and McNair, R. IEEE J., QE-7, 253 (1971).

4. Cohn, D. B. APPL. PHYS. LETTS., 21, 343 (1972).

5. Champaque, L. APPL. PHYS. LETTS., 23, 158 (1973).

6. Basov, N. G.; Danilychev, V. A.; Ionin, A. A.; Kovsh, I. B.; and Sobolev, V. A. KVANTOVAYA ELEKETRONIKA, 1, 2527 (1974).

7. Center, R. E. IEEE J., QE-10, 208 (1974).

8. Mann, M. M. AIAA PAPER No 75-34 (1975).

9. Basov, N. G.; Danilychev, V. A.; Ionin, A. A.; Kazakevich, V. S.; Kovsh, I. B.; Poletayev, N. L.; Sobolev, V. S.; and Khasenov, M. U. FIAN Preprint, Moscow, No 6, 1977.

10. Lacina, W. B., and McAllister, G. L. IEEE J., QE-11, 235 (1975).
11. Treanor, C. E.; Rich, J. W.; and Rehm, R. G. J. CHEM. PHYS., 48, 1728 (1968).

12. Basov, N. G.; Dolinina, V. I.; Suchkov, A. F.; and Urin, B. M. FIAN Preprint, Moscow, No 9, 1977.

13. Lobanov, A. N., and Suchkov, A. F. FIAN Preprint, Moscow, No 8, 1977.

14. Basov, N. G.; Danilychev, V. A.; Ionin, A. A.; Kerimov, O. M.; Kovsh, I. B.; and Poletayev, N. L. PIS'MA V ZHTF, 2, 817 (1976).

Institute of Physics imeni P. N. Lebedev,
USSR Academy of Sciences, Moscow
[154-3024]

Submitted 4 August 1978

PHYSICS

UDC: 621.378.33

STUDY OF A COOLED ELECTROIONIZATION CO LASER. II. LASER ACTION EMPLOYING MIXTURES OF CO AND BUFFER GASES

Moscow KVANTOVAYA ELEKTRONIKA in Russian Vol 6,No 6, Jun 79 pp 1215-1222

[Article by N. G. Basov, V. A. Danilychev, A. A. Ionin, V. S. Kazakevich, I. B. Kovsh, and N. L. Poletayev]

[Text] The authors have studied threshold, energy, temporal and spectral characteristics of a cryogenic pulsed electroionization CO laser employing mixtures of CO with helium and nitrogen. The active volume of the experimental laser is ~5 l, excitation time 30-300 microseconds, density of working gas $\leqslant$ 1.5 Amagat units. The authors show that cooling of the active medium to temperatures of 80-100 °K makes it possible to boost gain to 1.5 x 10^{-2} cm^{-1}, energy output to ~100 J/(l · Amagat), and efficiency to 35%. Radiation energies of ~250 J with a density of 0.5 Amagat unit and 400 J with a density of 1.5 Amagat units were obtained. Laser action is observed within the spectral range 4.95-5.5 microns. With an increase in pump energy and concentration of buffer gas, the generation spectrum shifts to the short-wavelength region. A decrease in concentration of CO in a nitrogen mixture to 2.5% with fixed excitation pulse duration of ~100 microseconds leads to increased radiation pulse duration (at half-height) from ~100 microseconds (pure CO) to ~3 milliseconds. The authors make a comparison of the results of theoretical calculations and the experimental data of other authors.

Experimental investigations performed in our study [1] indicated that an electroionization laser (EIL) employing pure carbon monoxide cooled to a temperature of ~100°K does not produce the high values of specific energy output and laser efficiency predicted by theory [2]. Further experiments on a CO-EIL were perfomed with the employment of mixtures of CO with buffer gases -- helium and nitrogen.

As we know, the addition of helium to CO does not alter the character of distribution of electrical excitation energy between degrees of freedom of molecules of CO, leading only to a decrease in the optimal value of reduced

field intensity E/N in comparison with pure carbon monoxide [3]. Nitrogen, the vibrational quantum of which insignificantly exceeds the vibrational quantum of carbon monoxide, while the section of excitation of vibrational levels by an electron impact almost entirely coincides with the excitation section of CO [4] in the range of electrical fields employed in electroionization excitation of a CO laser, can serve as a reservoir of vibrational energy for CO. The influence of He and N_2 on VT-relaxation of energy of molecules of CO in the investigated range of excitation durations

$$\tau_{возб} \leq 100\ msc \ll \tau^{VT}_{CO-He},\ \tau^{VT}_{CO-N_2} \quad [5]$$

is negligibly small.

In this study we investigated the influence of helium and nitrogen on excitation modes and generation characteristics of a pulsed CO-EIL. Experiments were performed on a laser unit with an active volume of ~5 l, as described in [6, 7].

1. Parameters of CO-EIL Employing Helium Mixtures

Measurement of the dependences of discharge input energy on field intensity in the discharge gap indicated that they are, just as in pure carbon monoxide, quadratic in nature, typical for an electroionization discharge (Figure 1). Just as in a CO_2-EIL [8, 9], with a fixed field intensity specific energy input with the presence of helium in the mixture is greater than in helium-free mixtures, which is due to the greater electron drift velocity values in mixtures with helium.

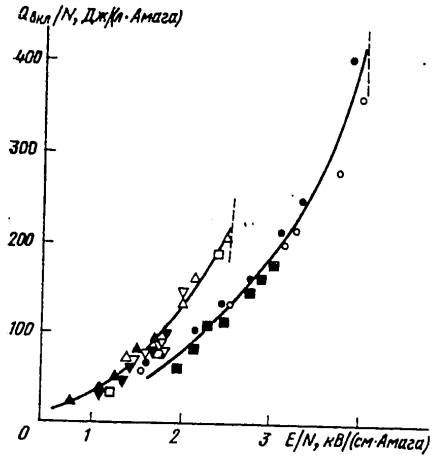

Figure 1. Dependence of Discharge Specific Energy Input on Reduced Initial Field Intensity for Various Mixtures

CO : N_2=1 : 0 (○); 1 : 2 (□); 1 : 6 (●) ($\tau_{возб}$=30 microseconds;
CO : He=1 : 1 (△); 1 : 3 (▽); 1 : 6 (▲); 1 : 12 (▼) и
CO : N_2 : He — 1 : 6 : 7 (■) $\tau_{возб}$=100 microseconds; N=

0.5 Amagat unit, T~100°K, C=18 mfd; the dashed line indicates discharge gap breakdown

The presence of helium in the laser mixture appreciably decreases maximum electrical field and discharge gap specific energy input values due to a decrease in electrical strength of the gas. For example, when the CO is 50% diluted with helium, maximum specific energy input value is ~200 J/(1 · Amagat), and for a CO:He=1:6 mixture -- only 100 J/(1 · Amagat), while for pure CO this value is 400 J/(1 ·Amagat).

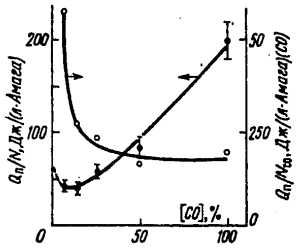

Figure 2. Dependence of Threshold Pump Energy on CO Concentration in CO-He Mixtures

N=0.5 Amagat; T=80°K; $\alpha_{\pi}=4\cdot10^{-3}$ cm^{-1}

With an increase in CO concentration there is an increase in reduced pumping energy Q_{π}/N required to reach the laser action threshold (Figure 2). This is connected with the fact that in order to reach laser action it is necessary to put in a specific energy per unit of carbon monoxide partial density N_{CO} [10]. It is evident from Figure 2 that the value of Q_{π}/N_{CO} is ~200-250 J/(1 ·Amagat) (CO) for mixtures with a 10-100% carbon monoxide content, or converted to CO partial pressure ~1.0-1.25 J/(1 ·mm Hg) (CO). This threshold energy value satisfactorily matches the theoretical estimates given in [10] for a mixture of CO with an inert gas. An appreciable increase in Q_{π}/N_{CO} with small CO concentrations is evidently connected with a decrease in the number of active particles and a consequent decrease in gain at a specified pumping energy level.

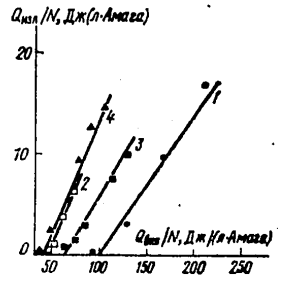

Figure 3. Dependence of Radiation Energy on Specific Pumping Energy for Mixtures CO:He=1:1 (1), 1:12 (2), 1:3 (3), 1:6 (4); N=0.5 Amagat, T=80°K, C-18 mfd

Measurements of radiation energy and laser efficiency of a CO-EIL were performed with varying CO content in laser mixtures (Figure 3). A comparison of experimental figures for pure carbon monoxide [1] and mixtures of carbon dioxide and helium indicates that the addition of helium prevents achieving a substantial increase in specific energy output as a consequence of decrease in maximum energy inputs. However, an increase in helium concentration in the laser mixture leads to an appreciable increase in differential laser efficiency (see Figure 3). For example, a shift from pure carbon monoxide to a CO:He=1:6 mixture increases differential efficiency from ~10 to ~25%. The greatest efficiency for mixtures with helium (not differential) was obtained with this same mixture at a density of 0.5 Amagat unit and comprised ~15% with energy output of ~15 J/(1 · Amagat) (an efficiency of approximately 3% was achieved for pure CO with the same density).

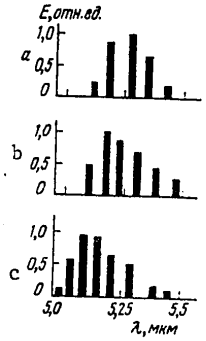

Figure 4. Distribution of Radiation Energy Across Laser Action Spectrum of CO-EIL Employing Mixtures of CO:He=1:0 (a), 1:1 (b) and 1:6 (c); N=0.5 Amagat,

---

The possibility of obtaining for helium mixtures a higher efficiency than with pure carbon monoxide may be due to a number of causes. In the first place employment of helium makes it possible substantially to increase reduced pumping energy $Q_{\text{вкл}}/N_{CO}$, which reaches, for a CO:He=1:6 mixture for example, a value of ~700 J/(1 · Amagat) (CO), and consequently to ensure stronger vibrational excitation of the CO. Secondly, an increase in efficiency may be connected with lower initial gas temperature (T~80°K), due to the greater thermal conductivity of helium-containing mixtures (gas cooling takes place due to withdrawal of heat to the cold walls of the laser chamber), as well as removal of kinetic energy to the buffer gas from CO molecules, energy released in the excitation and vibration-vibration exchange processes. Finally, one possible reason may be more efficient excitation of vibrational levels of CO molecules in an electrical discharge taking place in helium mixtures.

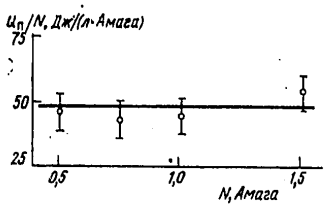

Figure 5. Dependence of Pumping Threshold Energy $Q_п$ /N on Density of Laser Mixture CO:N_2=1:6 when T=100°K; $\alpha_п = 4 \cdot 10^{-3}$ cm^{-1}; $(E/N)_п \sim 1.6$ kV/(cm·Amagat)

Spectral data (Figure 4) do not indicate an increase, with increased helium content, of efficiency of pumping molecules of carbon dioxide in a CO mixture. With an increase in helium concentration with a fixed pumping energy point above the threshold value, the laser action spectrum shifts into the short-wavelength region, whereby laser action is observed at low transition V→V-1=4→3 with a wavelength shorter than 5 microns. A similar effect of displacement of the laser action spectrum into the short-wavelength region is also observed with a fixed composition of the CO-He working gas mixture, when specific pumping energy increases. Such a shift, as was noted in [1], is connected with growth in the population density of the lower vibrational levels of CO and is caused by increase in intensity of vibrational excitation of carbon monoxide molecules.

Investigation of the radiation pulse shape for CO-He mixtures did not indicate that change in the concentration of carbon monoxide in helium mixtures exerts appreciable influence on laser action dynamics. In fact the role of helium boils down to increasing electron temperature and decreasing, caused by this, parameter E/N values optimal for exciting vibrational levels. Helium, being an elemental gas, does not provide for carbon monoxide a vibrational energy reservoir or drain, and development of laser action in a CO-He mixture is determined only by the properties of the CO molecules themselves (in that range of pumping pulse durations where

$$\tau^{VT}_{CO-He} \gg \tau_{возб}).$$

2. CO-EIL Employing Nitrogen-Containing Mixtures

The employment of nitrogen as a buffer gas made it possible substantially to increase energy input into volume discharge in comparison with helium mixtures. Maximum field intensity and specific energy input values for CO-N_2 mixtures are close to analogous parameters for a cooled CO-EIL employing pure carbon monoxide (see Figure 1). The maximum initial reduced field intensity value for nitrogen-containing mixtures under experimental conditions was ~4.5 kv/(cm · Amagat), and for CO:He=1:(1-12) mixtures, for example, it did not exceed 2.5 kv/(cm · Amagat). The energy input maximally attainable for CO-N_2 mixtures depended on gas density and was ~400 J/(l · Amagat) at N=0.5 Amagat unit and (~250 J/(l · Amagat) at N=1.5 Amagat units.

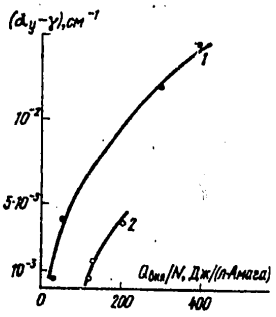

Figure 6. Dependence of Gain (with Accuracy to Nonresonant Losses) on Discharge Energy Input, for a Mixture CO:N_2=1:6 (1) and pure carbon monoxide (2); N=0.5 Amagat unit, T=100°K

Reduced threshold pumping energy $Q_{\text{п}}/N$ in laser mixtures with a buffer gas, just as in pure carbon monoxide, did not depend on density of the working gas mixture (Figure 5). However, the absolute value of $Q_{\text{п}}/N$ ($\alpha_{\text{п}} \sim 4 \cdot 10^{-3}$ cm^{-1}) in the described excitation mode proved to be approximately half that of a mode with excitation by short pulses with a duration of $\tau_{\text{возб}} \sim 0.2$ mcs ($\alpha_{\text{п}} \sim 5 \cdot 10^{-3}$ cm^{-1}) [11]. Apparently this discrepancy is caused by the less effectiveness of excitation of vibrational levels of a CO molecule in high intensity fields characteristic of short pulse mode [11].

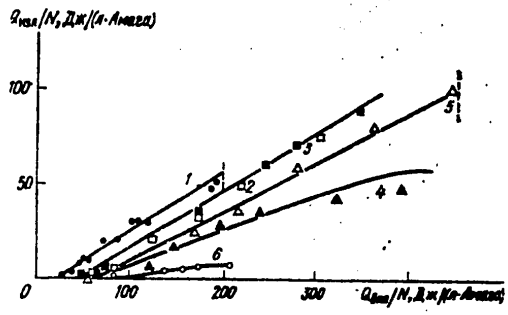

Figure 7. Dependence of Specific Radiation Energy on Specific Energy Input for Mixtures:

CO : N_2 : He = 1 : 6 : 7 (1); CO : N_2 = 1 : 10 (2); 1 : 19 (3); 1 : 39 (4); 1 : 6 (5) и 1 : 2 (6);

N=0.5 Amagat; T=100°K, $\tau_{\text{возб}} \sim$ 100 microseconds; the dashed line indicates discharge gap breakdown

With an increase in content of carbon monoxide in the $CO-N_2$ mixture the threshold pumping energy increases, just as in helium mixtures. Gain α_y, measured by threshold characteristics, increases with increase in pumping energy and reaches a value of $\sim 1.5 \cdot 10^{-2}$ cm^{-1} for a $CO:N_2=1:6$ mixture (with a specific energy input of 400 J/(1 · Amagat), which is twice the gain for pure carbon monoxide with the same energy input (Figure 6).

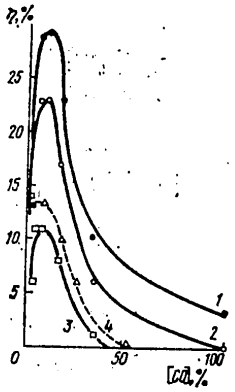

Figure 8. Dependence of CO-EIL Laser Action Efficiency on Concentration of CO in Nitrogen (1-3) and helium (4) mixtures for different specific energy inputs: $Q_{вкл}/N \approx 350$ (1), 200 (2) and 100 J/(1 · Amagat) (3, 4). N=0.5 Amagat, $\alpha_y = 4 \cdot 10^{-3}$ cm^{-1}; $T \approx 10°K$

$CO-N_2$ laser mixtures with a 5-15% carbon monoxide content proved optimal from an energy standpoint (Figure 7). Maximum specific energy output with a density of N=0.5 Amagat unit comprised ~100 J/(1 · Amagat) for them, while radiation energy was ~250 J per pulse. The presence of helium in a nitrogen mixture $CO:N_2:He=1:6:7$ appreciably increases laser action efficiency, which in this case reaches ~30% with an energy input of ~100 J/(1 · Amagat). A comparison of laser action efficiency for $CO-N_2$ and CO-He mixtures with identical specific energy input indicates that for a helium mixture efficiency is 20-30% higher than for nitrogen (Figure 8). This difference is connected with the fact that a portion of the discharge input energy remains at the vibrational levels of nitrogen and is not transmitted to the CO molecules. Employment of nitrogen, however, makes it possible to achieve substantially greater discharge energy inputs and consequently greater energy outputs and efficiency than in helium mixtures.

The greatest radiation energy of 400 J (with specific energy output of ~60 J/(1 · Amagat)) was obtained utilizing a $CO:N_2=1:6$ mixture with a density of 1.5 Amagat units (Figure 9). Maximum efficiency value for nitrogen mixtures was ~30-35%.

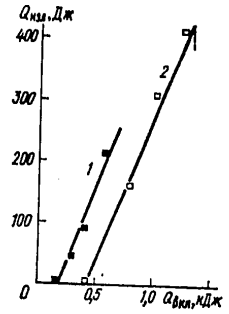

Figure 9. Dependence of CO-EIL Complete Radiation Energy on Energy Put Into an Active Volume V≈5 l where T=100°K; $\tau_{имп}$=70 mcs; N=0/75 (1) and 1.5 Amagat (2); C=18 (1) and 6 mfd (2)

Adding nitrogen to carbon monoxide leads to a substantial increase in duration of laser action. While in pure carbon monoxide laser pulse duration (at half-height) when $\tau_{имп}$≈30 mcs is ~100 mcs, in a CO:N_2=1:6 mixture, with the same pumping mode, it is 200 mcs, and with a CO content of 2.5% in the mixture -- 3 ms at half-height (Figure 10), while in the latter instance efficiency is still fairly high (~15%). Increase in laser action duration with the addition of N_2 to the CO is evidently linked with excitation of nitrogen vibrational levels in the discharge and subsequent transfer of excitation energy to the CO vibrational levels, which are characterized by a large time constant [12]. Such an increase in duration of laser action was observed, for example, in TEA-CO lasers [13].

Just as in pure carbon monoxide, duration of laser action in mixtures increases with pumping intensity, while a radiation power spike is recorded at the moment excitation terminates. In addition, in mixtures with small CO content (≲5%) complete suppression of laser action occurs during the pumping process, suppression which subsequently occurs with a delay of several tens of microseconds (see Figure 10). Evidently appearance of the first pulse is connected with direct excitation of the CO molecule by an electron impact, and cessation of laser actions -- with deexcitation of high vibrational levels by an electron impact [1], and subsequent laser action -- with transfer of excitation from the N_2 to the CO.

The radiation spectrum of CO-EIL employing nitrogen mixtures lies in a shorter-wavelength band than with pure CO (Figure 11). With an increase in pumping energy, just as in pure CO [1] and CO-He mixtures, lower vibrational levels begin to take part in laser action, and the laser action spectrum and its maximum shift toward shorter wavelengths.

The experiments showed that the addition of helium and nitrogen to carbon monoxide substantially increases energy output and laser action efficiency in comparison with a laser employing pure carbon monoxide. A high degree of laser action efficiency is observed with a concentration of CO ~5-15%. In order to attain high radiation energies with specific power outputs of

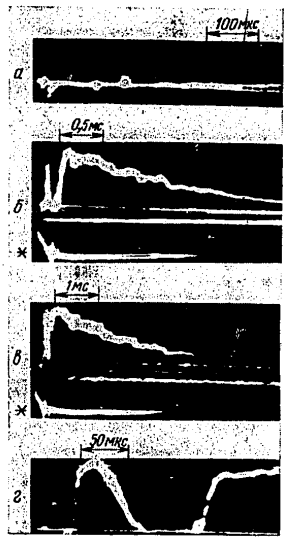

Figure 10. Oscillograms of CO-EIL Radiation Pulses With a Mixture of CO:N_2= 1:39: $Q_{вкл}$/N=60 (а), 150 (б) and 200 J/(1 · Amagat) (в, г); N=0.5 Amagat, T=100°K, $\tau_{возб} \approx 150$ mcs (lower lines in б, в -- pumping signal)

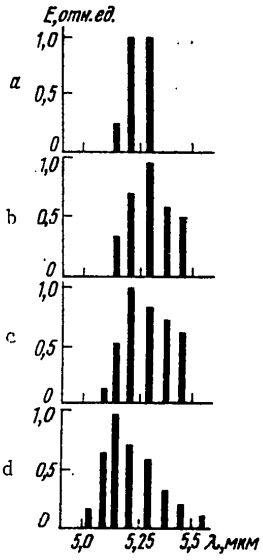

Figure 11. Distribution of Radiation Energy Across CO-EIL Laser Action Spectrum for Pumping Energy: $Q_{вкл}$/N=50 (a), 100 (b), and 240 J/(1 · Amagat) (c); mixture CO:N_2= 1:6, N=0.5 Amagat, T=100°K

~100 J/(1 · Amagat) (300 J/(1 ·atm)) and efficiency ~30-35%, it is necessary to employ nitrogen-containing mixtures. Change in the composition of the laser mixture and excitation energy affects the dynamics and laser action spectrum of a CO-EIL, making it possible to control radiation duration in the range ~30 mcs-3 ms, and spectral composition of radiation in the region ~5.0-5.5 microns.

Comparison of the experimental data obtained in this study with theory is complicated in connection with the fact that there is lacking in the literature sequential calculations of the laser action characteristics of a CO-EIL for a broad range of working gas mixture parameters and pumping modes. An approximate analytical theory of "scaling" CO-EIL energy characteristics [10] leads to dependences of delay time and laser action efficiency on the conditions of excitation, which qualitatively match with experimental figures, but the calculated values τ_3 prove to be an order of magnitude less, and efficiency two to three times those values measured in our study. The conclusion reached in [2] on the basis of numerical calculations that the gain in pure carbon monoxide is greater than in a CO-N_2 mixture with the same energy input contradicts experimental figures (see Figure 6). The absence of a dependence of laser action characteristics of a CO-EIL on temperature with retention of reduced pumping power, predicted by calculations [10, 14], is also in contradiction to experiment. The only quantity presently calculated with sufficient accuracy is threshold pumping energy at an active medium temperature of ~100°K. Calculations of laser action spectra and dynamics for CO-EIL employing CO-He and CO-N_2 mixtures are practically lacking in the literature.

In experimental study [15], which discusses development of a CO-EIL with a small (~1.5 l) cooled active volume, the results of parametric investigations are not presented; the authors indicate only the maximum energy characteristics of the designed laser, obtained with maximum achievable energy input. Our investigations were conducted at lower $Q_{вых}$ values, but extrapolation of relations $Q_{изл}$ ($Q_{вых}$) and efficiency ($Q_{вых}$) to quantities $Q_{вых}^{max} \approx 600$ J/(1 · Amagat) [15] for a mixture CO:N_2=1:6 (N=0.75; 1.5 Amagat units) leads to practically the same values of specific energy output and efficiency as in the indicated study. Such a conformity is not observed for mixtures of CO with inert gases; the efficiency value measured for a CO-He mixture is lower than the same value for the CO-Ar mixture obtained in [15].

The maximum efficiency value (~15%) obtained in [16] for a nitrogen mixture is considerably less than the laser action efficiency observed in [6, 15] and in our experiments. Apparently, as the authors of [16] note, this is connected with nonuniform cooling of the laser active medium. In a subsequent study by these same authors [17], an efficiency of ≈35% was obtained for CO-N_2 mixtures, which satisfactorily agrees with the results of our experiments [6]. Analysis of the results obtained on cryogenic units with a large excitation volume [6, 7, 17, 18] indicates that in designing high-output pulsed CO-EIL one can expect in free laser action mode an efficiency of ≈30-40% and specific energy output of ~100-200 J/(1 · Amagat).

Our experimental investigations of the energy, spectral and temporal characteristics of CO-EIL enable us to conclude that existing electrical-excitation high-pressure CO laser theory does not permit one to make accurate calculations of the output characteristics of CO-EIL. Developed calculation methods require improvement, and also needed are precise measurements of constants determining the processes of excitation and relaxation of vibrationally excited CO molecules. The experimental data amassed in the course of studies [1, 6, 7, 9, 11, 17-20] permit one to formulate sufficiently accurately demands on CO-EIL pumping mode and active medium parameters ensuring the requisite radiation characteristics (energy, efficiency, pulse duration, spectrum), and consequently can serve as a basis for designing pulsed CO-EIL with specified output parameters.

BIBLIOGRAPHY

1. Basov, N. G.; Danilychev, V. A.; Ionin, A. A.; Kazakevich, V. S.; Kovsh, I. B.; and Poletayev, N. L. KVANTOVAYA ELEKTRONIKA, 6, 1208 (1979).

2. Basov, N. G.; Dolinina, V. I.; Suchkov, A. F.; and Urin, B. M. FIAN Preprint, Moscow, No 1, 1976.

3. Lobanov, A. N., and Suchkov, A. F. FIAN Preprint, Moscow, No 8, 1977.

4. Mak-Daniel', I. "Protsessy stolknoveniy v ionizirovannykh gazakh" [Collision Processes in Ionized Gases], Moscow, Mir, 1967.

5. Sobolev, N. N., and Sokovikov, V. V. UFN, 110, 191 (1973).

6. Basov, N. G.; Danilychev, V. A.; Ionin, A. A.; Kovsh, I. B.; Kazakevich, V. S.; Poletayev, N. L.; Sobolev, V. A.; and Khasenov, M. U. FIAN Preprint, Moscow, No 6, 1977.

7. Basov, N. G.; Danilychev, V. A.; Ionin, A. A.; Kazakevich, V. S.; Kovsh, I. B.; and Poletayev, N. L. PIS'MA V ZHTF, 3, 385 (1977).

8. Basov, N. G.; Belenov, E. M.; Danilychev, V. A.; Kerimov, O. M.; Kovsh, I. B.; and Suchkov, A. F. ZHTF, 42, 2540 (1972).

9. Basov, N. G.; Danilychev, V. A.; Ionin, A. A.; Kovsh, I. B.; and Sobolev, V. A. KRATKIYE SOOBSHCHENIYA PO FIZIKE, FIAN, No 6, 3,(1974).

10. Lacina, W. B., and McAllister, G. L. IEEE J., QE-11, 235 (1975).

11. Basov, N. G.; Danilychev, V. A.; Ionin, A. A.; Kerimov, O. M.; Kovsh, I. B.; and Poletayev, N. L. PIS'MA ZHTF, 2, 817 (1976).

12. Stephenson, J. S. APPL. PHYS. LETTS, 22, 576,(1973).

13. Cohn, D. B. IEEE J., QE-10, 459 (1974).

14. Center, R. E., and Caledonia, G. E. J. APPL. PHYS., 48, 2215 (1975).

15. Mann, M. M.; Rice, D. K.; and Eguchi, R. G. IEEE J., QE-10, 682 (1974).

16. Center, R. E. IEEE J., QE-10, 682 (1974).

17. Boness, M. J. W., and Center, R. E. J. APPL. PHYS., 48, 2705 (1977).

18. Mann, M. M. AIAA J., 14, 549 (1976).

19. Basov, N. G.; Danilychev, V. A.; Ionin, A. A.; Kovsh, I. B.; and Sobolev, V. A. KVANTOVAYA ELEKTRONIKA, 1, 2527 (1974).

20. Basov, N. G.; Danilychev, V. A.; Ionin, A. A.; Kerimov, O. M.; Kovsh, I. B.; Suchkov, A. F.; Urin, B. M.; and Khasenov, M. U. KVANTOVAYA ELEKTRONIKA, 3, 1145 (1976).

Physics Institute imeni P. N. Lebedev
of the USSR Academy of Sciences, Moscow
[154-3024]

Submitted 4 August 1978

PHYSICS

UDC: 621.378.33

RAMAN HYDROGEN LASER FOR EFFICIENT COHERENT SUMMATION OF NANOSECOND LIGHT PULSES

Moscow KVANTOVAYA ELEKTRONIKA in Russian Vol 6 No 6, Jun 79 pp 1329-1331

[Article by N. G. Basov, A. Z. Grasyuk, Yu. I. Karev, L. L. Losev, and V. G. Smirnov]

[Text] The authors built and investigated a high-efficiency Raman laser utilizing stimulated Raman scattering by rotational levels in gaseous hydrogen. Under conditions of saturated amplification of external signal in the Raman amplifier, the authors obtained coherent summation of 50 neodymium laser beams with an efficiency of 70% into a single spatially coherent light beam at the first Stokes frequency of ν_c=8856 cm^{-1}.

Extremely rigid demands pertaining to divergence and energy density on the target are imposed on modern laser systems designed, for example, for thermonuclear synthesis, demands which are very difficult to meet.

The author of [1] presents a new way to solve this problem, the basic idea of which is as follows: an initial multichannel laser unit is employed as a pump source for Raman lasers (RL), and converted radiation is concentrated on the target. This substantially reduces the demands imposed on the pumping source: it must only ensure specified energy and power requisite for stimulated Raman scattering with a fairly large (5-10 mrad) divergence. Small divergence and high energy density are achieved by pump frequency conversion in RL. The advantage of such an arrangement over the conventional generator-amplifier arrangement is obvious. Utilization of high-efficiency RL as final stages of a multichannel unit can not only increase laser radiation brightness and eliminate the possibility of self-excitation due to reflection of radiation from the target, but can also substantially (tens to hundreds of times) reduce the number of light beams the energy of which must be concentrated on the target.

This article deals with development and investigation of an RL-amplifier for efficient coherent summation of a large number of light beams of a neodymium laser operating in the band of nanosecond pulses. The term "coherent summation" signifies that as a result of nonlinear interaction between laser

radiation and environment, n pumping beams, each of which has a section S_H, are transformed into one spatially coherent RL beam with a section S_C, the energy density of which is $n\eta S_H/S_C$ times that of the pump (η -- efficiency of conversion).

As was demonstrated as early as 1966 [2], stimulated Raman scattering [SRS] at rotational levels with a frequency shift of Ω=587 cm^{-1} is possible in gaseous hydrogen. Consequently maximum efficiency of pump conversion at a frequency of ν_H=9443 cm^{-1} (Nd laser) is $\eta_{max}=(\nu_H-\Omega)/\nu_H\approx 94\%$. Nevertheless up to the present time there has not been a single study in which this type of SRS has been investigated as a method of efficient frequency conversion of laser radiation. We selected gaseous hydrogen as an active medium on the basis of preliminary experiments which indicated that in this medium one can convert up to 50% of pump energy into one Stokes component with a frequency ν_C=8856 cm^{-1}. In addition, the value of the gain measured by us for SRS at rotational levels with H_2 pressure from 2 to 8 atm proved sufficiently high ($g\approx 10^{-3}$ cm/M w) to effect frequency conversion at a small active medium length L. Indeed, gain increment b=g [cm/M w] I_H [M w/cm^2] L [cm] for efficient conversion should be in the order of 30-50 and, consequently, for gigawatt pumping intensities I_H length $L\approx$30-50 cm.

The range of duration of pump pulses determined the design of the RL, which should operate under conditions of saturated external signal amplification. These conditions were first investigated in [3], where it was shown that in a Raman amplifier one can achieve 100% quantum output if input signal intensity comprises several percent of pumping intensity.

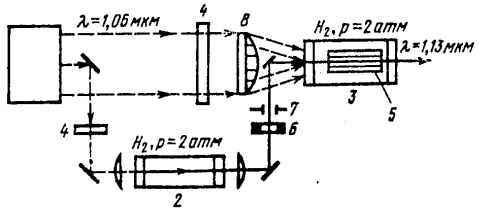

Figure 1. Diagram of Experimental Unit

Figure 1 contains a simplified diagram of an experimental setup. It contains pumping source 1 (neodymium laser consisting of a driving oscillator, electrooptical shutter, preamplifier and amplifier), a combination converter (oscillator 2 and amplifier 3) and recording equipment. Rotation of pumping polarization was effected with Fresnel parallelepipeds 4. The driving oscillator operated in a mode with Q modulation with a passive shutter and emitted linear-polarized light pulses of duration $\tau_H\approx$30 ns. The electrooptical shutter served for shaping a pulse of duration $\tau_H\approx$3 ns. The preamplifier and amplifier operated on a two-way setup, whereby the output radiation parameters of the neodymium laser had the following values: energy E_H=1.5 J; pulse duration τ_H=3 ns; divergence at half energy level θ=3 mrad; spectral width $\Delta\nu_H\lesssim$0.05 cm^{-1}.

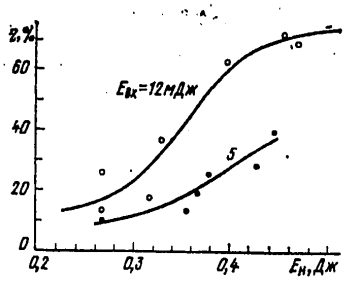

Figure 2. Dependence of Conversion Efficiency in a Raman Amplifier on Pump Energy.

A vessel L=1 m in length, filled with hydrogen to a pressure of 2-8 atm, was employed as Raman oscillator (input signal source). The Raman amplifier was designed in the form of a vessel 70 cm in length, inside which was placed half-meter lightguide 5 measuring 0.5 x 0.5 cm in section. In order to equalize pressures in both vessels, they were connected by a tube.

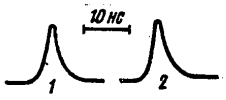

Figure 3. Pump (2) and Converted Radiation (1) Pulses at Raman Amplifier Output

A portion of the pump energy was drawn off by a mirror 1 cm in diameter and focused into the oscillator vessel with a lens with a focal length F=1 m. Output radiation through selective filters 6, attenuating the second Stokes frequency 100-fold, and diaphragm 7, measuring 0.5 x 0.5 cm, were directed with the aid of lenses and two mirrors into the Raman amplifier lightguide. Raman amplifier pumping was effected with square-section light beams measuring 0.5 x 0.5 cm, each of which was aimed into the end aperture of the lightguide. The number of beams totaled 50, and maximum energy contained in each comprised $E_{Hп}$ =10 mJ. Such pumping of a Raman amplifier with the aid of screen 8 4] can be viewed as a model of RL excitation with utilization of a large number of parallel pumping source terminal amplifiers operating from one driving oscillator.

If pressure in the vessels was 8 atm, and input signal energy with first Stokes frequency ν_c was 2-3% of maximum energy value of all pump beams (E_H=0.5 J), efficiency of conversion in the amplifier reached 50%. However,

almost two thirds of output radiation energy was contained in the second Stokes component with a frequency ν_{cc}=8269 cm^{-1}. A decrease in input signal intensity improves this relationship in favor of the first Stokes frequency, but conversion efficiency drops. It proves possible to reduce to a minimum radiation energy output at a frequency of ν_{cc} and its negative influence on conversion efficiency by reducing gain g with decrease in pressure in the vessels to 2 atm.

Test results are shown in Figure 2. With an accuracy to 5 mJ, converted radiation does not contain the second Stokes component, while maximum efficiency of conversion into the first amount to 70%. The shape and duration of pumping pulses and converted radiation practically coincide thereby (Figure 3).

The principal pumping and converted radiation characteristics are presented below.

	Pumping Source	RL With H_2
Wavelength, microns	1.06	1.13
Number of beams	50	1
Beam section, mm	5 x 5	5 x 5
Pulse duration, ns	3	3
Divergence (by level of half-energy), mrad	3	1
Energy, J	0.5	0.36
Power, Gw	0.165	0.12
Energy density, J/cm^2	0.04	1.45
Intensity, Gw/cm^2	$1.4 \cdot 10^{-2}$	0.48

With RL input signal energy $E_{вх} \approx$ 12-14 mJ, a brightness increase of $B_{кл}/B_H \approx 300$ was achieved.

Thus in these experiments was achieved for the first time with a high efficiency (η =70%) coherent summation of the energy of 50 beams of a neodymium laser operating in nanosecond pulse mode. The obtained results suggest that the development and improvement of such RL opens up the possibility for their utilization in laser systems of the Del'fin type, designed for obtaining laser thermonuclear synthesis [1].

The authors express thanks to A. N. Orayevskiy for stimulating discussions.

BIBLIOGRAPHY

1. Basov, N. G. Preprint P. N. Lebedev Physical Institute, Moscow, 1978, No 153.

2. Minck, R. W.; Hagenlocker, E. E.; and Rado, W. G. PHYS. REV. LETTS, 17, 229 (1966).

3. Grasyuk, A. Z.; Zubarev, I. G.; Mishin, V. I.; and Smirnov, V. G. KVANTOVAYA ELEKTRONIKA, N. G. Basov, editor, No 5 (17), 27 (1973).

4. Grasyuk, A. Z.; Yefimkov, V. F.; and Smirnov, V. G. PTE, No 1, 174 (1976).

Physics Institute imeni P. N. Lebedev
of the USSR Academy of Sciences, Moscow
[154-3024]

Submitted 28 February 1979

SCIENTISTS AND SCIENTIFIC ORGANIZATIONS

FIFTIETH BIRTHDAY OF FEDOR VASIL'YEVICH BUNKIN

Moscow KVANTOVAYA ELEKTRONIKA in Russian Vol 6 No 6, Jun 79 page 1352

[Article by S. A. Akhmanov, A. I. Barchukov, M. F. Bukhenskiy, V. G. Veselago, V. S. Zuyev, N. V. Karlov, P. P. Pashinin, G. P. Shipulo, V. V. Savranskiy, and I. N. Sisakyan: "Fedor Vasil'yevich Bunkin (In Honor of His 50th Birthday)"]

[Text] By ukase of the Presidium of the USSR Supreme Soviet dated 22 January 1979, Fedor Vasil'yevich Bunkin, Corresponding Member of the USSR Academy of Sciences, was awarded the Order of the Red Banner of Labor for his contributions toward the development of radiophysics and electronics, training of personnel, and in connection with his 50th birthday.

F. V. Bunkin was born on 17 January 1929 in the family of an engineer-geodesist. Upon graduating from the Physics-Technical Faculty at Moscow State University imeni M. V. Lomonosov (1952), he took a position at the Physics Institute imeni P. N. Lebedev of the USSR Academy of Sciences. He defended his candidate's dissertation in 1955 and his doctoral dissertation in 1963. He was elected corresponding member of the USSR Academy of Sciences in 1976.

The name F. V. Bunkin is closely linked with the development and successes of radiophysics in this country. His work in the field of classic electrodynamics, statistical radiophysics and quantum electronics constitutes a major contribution toward theoretical radiophysics and toward solving many practical problems.

F. V. Bunkin formulated and solved the problem of bremsstrahlung of electrons in a strong electromagnetic field and developed a method of solving problems of radiation in anisotropic media. Of great theoretical and practical significance is research performed under his supervision on the interaction of powerful electromagnetic (laser) radiation with matter, as a result of which new physical effects were discovered: propagation of optical discharges in gaseous media in "slow burn" mode, low-threshold breakdown of gases by infrared radiation in the vicinity of solid targets, etc.

F. V. Bunkin combines scientific activity with scientific-organizational work. He is chairman of the USSR Academy of Sciences Scientific Council on the problem "Coherent and Nonlinear Optics," and is a member of the editorial board of the journal KVANTOVAYA ELEKTRONIKA. Fedor Vasil'yevich devotes much attention to training scientific personnel in his capacity as professor at the Moscow Physical-Technical Institute.

F. V. Bunkin is at the height of his creative powers. His inexhaustible energy, versatility of interests in the area of scientific quest, his high principles and demandingness of the scientist-Communist on himself, his colleagues and co-workers constitute a guarantee of continued fruitful activity.

We wish F. V. Bunkin continued health, good spirits and continued productive success in the development of Soviet science.
[154-3024]

CSO: 1862

END